NTNU – Trondheim
Norwegian University of
Science and Technology

Influence of marine growth on support structure design for offshore wind turbines

Live Salvesen Fevåg

Civil and Environmental Engineering
Submission date: June 2012
Supervisor: Michael Muskulus, BAT

Norwegian University of Science and Technology
Department of Civil and Transport Engineering

NORWEGIAN UNIVERSITY OF SCIENCE AND TECHNOLOGY
DEPARTMENT OF CIVIL AND TRANSPORT ENGINEERING

Report Title:	Date: 11.06.2012			
Influence of marine growth on support structure design for offshore wind turbines	Number of pages (incl. appendices): 109			
	Master Thesis	x	Project Work	
Name: Live Salvesen Fevåg				
Professor in charge/supervisor: Michael Muskulus				
Other external professional contacts/supervisors:				

Abstract:

This Master's thesis addresses the effects of marine growth on the design of a lattice tower substructure for an offshore wind turbine. Marine growth is the unwanted colonization of marine structures by marine organisms. The current standards prescribe a thickness of 100~mm whereas in the literature, layers up to 200~mm thick have been reported for structures in the North Sea.

Marine growth leads to increased wave loading on the structure. This is caused by the increased effective member diameter, as well as increased drag coefficient due to increased surface roughness. Marine growth also represents an additional non-structural mass, reducing the structural natural frequencies. Marine growth may increase flow instability and vortex shedding, but this has not been evaluated in this report. The effects of marine growth have been evaluated for the NOWITECH 10 MW reference turbine.

Alteration of the natural frequencies caused dynamic amplification when structural natural frequencies approached the nP-values of the rotor. The effect was most prominent for the local-modes natural frequencies, the modes including out-of-plane deformation of the bracing.

The relative importance of the increased hydrodynamic load and additional non-structural mass was investigated. It was concluded that both effects must be included in the model to describe the dynamic behaviour.

The fatigue lifetime of the K-braces was more sensitive to marine growth thickness than that of the X-braces. The X-brace fatigue lifetime gave the design lifetime for this particular design and marine growth lead to significant reductions in the fatigue lifetime. Marine growth would increase the lifetime in certain points. Thus, it is necessary to check the design also without marine growth.

Keywords:

1. offshore wind
2. marine growth
3. full-height lattice tower
4. local vibrations

Task description

Influence of marine growth on support structure design for offshore wind turbines

Offshore wind turbines for intermediary water depths (30-50m) are nowadays often built on top of jacket support structures adapted from the oil and gas industry. All submerged parts of the jacket are typically colonized by marine organisms (mussels, algae, seaweed) to a certain extent, that also varies in time. This changes the hydrodynamic properties (e.g., drag coefficients) and results in additional non-structural mass that needs to be accounted for in models. Current standards prescribe certain amounts of marine growth that should be used for designing offshore wind turbine support structures, but are they realistic? It is not really known what the influence of different degrees of marine growth on these jacket designs are.

The student will both work in cooperation with OWEC Tower AS (Bergen) on a commercial jacket design, as well as on the lattice support structure developed in our group for the 10 MW NOWITECH reference turbine, for which results can be freely published. Existing data on marine growth will be collected and typical patterns to be used for further analysis will be proposed. A theoretical model for a single vertical beam will be studied, in order to predict changes of joint fatigue lifetime with respect to the amount of marine growth and changes of the drag coefficient. Parametric studies shall be performed, varying the amount of marine growth globally and locally. Changes in eigenfrequencies and load distributions at the jacket bottom shall be studied. Finally, time-domain simulations shall be run for a few load cases, and conclusions about changes in fatigue damage due to marine growth shall be reached. The damage shall be compared to the predictions from the simple model. The analyses shall be conducted in FEDEM Windpower, and optionally in GL Garrad Hassan Bladed.

Abstract

This Master's thesis addresses the effects of marine growth on the design of a lattice tower substructure for an offshore wind turbine. Marine growth is the unwanted colonization of marine structures by marine organisms. The current standards prescribe a thickness of 100 mm whereas in the literature, layers up to 200 mm thick have been reported for structures in the North Sea.

Marine growth leads to increased wave loading on the structure. This is caused by the increased effective member diameter, as well as increased drag coefficient due to increased surface roughness. Marine growth also represents an additional non-structural mass, reducing the structural natural frequencies. Marine growth may increase flow instability and vortex shedding, but this has not been evaluated in this report. The effects of marine growth have been evaluated for the NOWITECH 10 MW reference turbine.

Alteration of the natural frequencies caused dynamic amplification when structural natural frequencies approached the nP-values of the rotor. The effect was most prominent for the local-modes natural frequencies, the modes including out-of-plane deformation of the bracing.

The relative importance of the increased hydrodynamic load and additional non-structural mass was investigated. It was concluded that both effects must be included in the model to describe the dynamic behaviour.

The fatigue lifetime of the K-braces was more sensitive to marine growth thickness than that of the X-braces. The X-brace fatigue lifetime gave the design lifetime for this particular design and marine growth lead to significant reductions in the fatigue lifetime. Marine growth would increase the lifetime in certain points. Thus, it is necessary to check the design also without marine growth.

Sammendrag

Denne masteroppgaven tar for seg de virkningene marin vekst kan ha på dimensjoneringen av et fagverksunderstell til en vindturbin til havs. Med marin vekst menes uønsket begroing av marine konstruksjoner. De aktuelle standardene anbefaler å bruke en tykkelse på 100 mm, mens det er rapportert opp til 200 mm tykke lag marin vekst på konstruksjoner i Nordsjøen.

Marin vekst fører til økte bølgelaster på fagverket. Dette skyldes at de effektive diameterne øker og at økt overflateruhet fører til at dragkoeffisienten øker. På grunn av den ekstra massen den marine veksten representerer, reduseres også konstruksjonens egenfrekvenser. Marin vekst kan øke virvelavløsning og virvelinduserte svingninger, men dette har ikke blitt behandlet. Virkningene av marin vekst har blitt evaluert for referanseturbinen NOWITECH 10 MW.

Når egenfrekvensene endret seg, ble det observert dynamisk resonans mellom dem og P-verdiene. Effekten var størst for de lokale egenmodene, de som fører til at avstivningene beveger seg ut av sideplanet.

Virkningene av økt bølgelast og økt masse ble målt opp mot hverandre. Begge effektene må tas hensyn til hvis den dynamiske responsen til konstruksjonen skal bli representert riktig.

Levetiden i X-knutepunktene var dimensjonerende for akkurat denne utformingen av fagverksunderstellet og marin vekst førte til en signifikant reduksjon av utmattingslevetiden. Marin vekst hadde større virkning på utmattingslevetiden i K-knutepunktene enn på levetiden i X-knutepunktene.

Marin vekst førte også til økt levetid i enkelte punkter. Dermed må det understrekes at understellet også må dimensjoneres uten marin vekst.

Preface

This Master's thesis was written for the Marine Civil Engineering Division at the Department of Civil and Transport Engineering, NTNU. It represents the full work load of the last spring semester of the five-year Master programme Civil and Environmental Engineering.

I would like to thank my supervisor Associate Professor Michael Muskulus for suggesting the topic and his guidance and advice. Also, I thank PhD Candidate Daniel Zwick for always taking the time to discuss new results, patiently answering my questions and suggesting new approaches when I was stuck in a dead end. Without his help, this report would have been a slim pamphlet!

I am also grateful that I was invited to attend the 9th Deep Sea Offshore Wind R&D Seminar in January. It was a very interesting introduction to the wind industry and the wind research community.

I would like to thank Associate Professor Øivind Arntsen for initiating a series of social meetings for the master students in the Marine Civil Engineering group. I hope that also future master students will have this opportunity to practice presentation skills (and eat free pizza).

Finally, I thank Karsten for helping me keeping the spirits up.

Trondheim, June 11th, 2012

Live Salvesen Fevåg

Contents

List of figures

List of tables

List of abbreviations and symbols

DNV		Det norske Veritas
FL		(distributed over the) full lenght
IEC		International Electrotechnical Commission
JONSWAP		Joint North Sea Wave Project
MG		marine growth
MGT		marine growth thickness
NOWITECH		Norwegian Reseach Centre for Offshore Wind Technology
SEC		section wise (distributed)
a	m	wave amplitude
d	m	water depth
f	Hz	frequency
f_D	N/m	drag term
f_I	N/m	inertia term
g	m/s^2	acceleration of gravity
k	1/m	wave number
k	N/m	structural stiffness
m	kg	mass
m	-	slope
u	m/s	velocity in x-direction
w	m/s	velocity in z-direction
A_γ	-	parameter in the JONSWAP spectrum
C_d	-	drag coefficient
C_m	-	inertia coefficient

D	m	cylinder diameter
D	-	fatigue damage
E	MPa	Young's modulus
F	N	drag force
H	m	wave height
H_S	m	significant wave height
I	m^4	area moment of inertia
I_t	%	wind turbulence intensity
K_C	-	Keulegan-Carpenter number
L	m	length
L_u	m	parameter in the Kaimal wind spectrum
N_{max}	-	fatigue life
Re	-	Reynolds number
T	s	period
T_p	s	peak period
U	m/s	wind speed
U_{10}	m/s	reference wind speed
α	-	power law exponent
γ		parameter in the JONSWAP spectrum
ϵ	-	phase angle
η	m	instantaneous wave elevation
λ	m	wave length
ν	m^2/s	kinematic viscosity
ρ	kg/m^3	mass density
σ	-	parameter in the JONSWAP spectrum
σ	Pa	stress
σ_U	m/s	standard deviation of wind speed
ω	1/s	angular frequency

Chapter 1

Introduction

1.1 Motivation

Energy extracted from offshore wind turbines offers an attractive opportunity in the search for climate-friendly energy supply. Offshore, wide areas are available, wind speeds are higher and the winds are more stable. Located offshore, the wind parks are also unobtrusive. The monopile is still the dominating substructure type, supporting 70 % of the offshore wind turbines [4]. An alternative is the jacket substructure, where the tower is mounted on top of a lattice structure, connected by a transition piece. This substructure concept is attractive as the wind turbines can be placed in deeper water and support larger rotors.

Jacket structures are well known from oil and gas industries, but wind turbine jackets have other characteristics and experience other loads. Important differences include that the jacket itself is much smaller and that the jacket members are more slender. The topside load is smaller and the loads from the rotating wind turbine are introduced.

Fatigue considerations are important for the design of jacket substructures. Cyclic loads include the harmonic load from the rotating wind turbine as well as wave loads. Welded nodes are fatigue-prone because of stress concentrations at the intersection points [1].

The NOWITECH 10 MW reference turbine has been developed at the Nor-

wegian Research Centre for Offshore Wind Technology. It is a three-bladed, horizontal axis wind turbine designed for a water depth of 60 m. Jacket substructures for wind turbines have successfully been installed in the North Sea, but the NOWITECH 10 MW reference turbine introduces a four-legged, full-height lattice tower as support structure. The major advantages are that the expensive and fatigue-prone transition piece is removed and that the total weight of the total support structure is expected to be smaller, compared to jacket structures [5].

Marine growth is the unwanted colonization of underwater surfaces of man-made structures by marine organisms. It may influence the reliability and performance of ships, buoys, piers, oil and gas platforms, or in our case: wind turbine substructures. In this report, biofouling and marine growth are two terms used to describe the same phenomenon.

Marine growth will influence the design of lattice structures in two ways. The hydrodynamic properties of the structure will change, leading to increased wave loading. The projected area subjected to wave loading as well as the drag coefficient will increase. Also, marine growth represents an additional non-structural mass, which will decrease the natural frequencies of the structure. This might move the natural frequencies closer to the loading frequencies, increasing the probability of resonance to occur.

Oldfield (ed.) investigated the relative importance of these two mechanisms by carrying out calculations on a typical North Sea steel jacket structure for oil and gas platforms [2]. The effect of increased hydrodynamic loading was found to be more important than the effect of increased dynamic amplification factor. It was also concluded that marine growth levels are important for the integrity of offshore structures, that the consequences of marine growth are more severe to fatigue design than ultimate limit state-considerations and that marine growth considerations are more important for slender jacket members.

Kjetså and Saaghus investigated local dynamics of the same lattice tower as considered in this report, as well as a jacket wind turbine substructure [6]. They conclude that local out-of-plane vibration modes are highly sensitive to changes in marine growth. Also, the joint fatigue lifetime is significantly reduced because of the increase in marine growth.

1.2 Objectives

The objectives of this thesis are

- To collect existing data on marine growth.
- To propose typical patterns of marine growth to be used in the analyses.
- To predict changes in joint fatigue lifetime with respect to the amount of marine growth and changes in the drag coefficient, by studying a single vertical beam.
- To do parametrical studies on the NOWITECH 10 MW reference turbine, varying the amount of marine growth globally and locally. The effect on natural frequencies, load distributions at the lattice tower bottom as well as changes in the fatigue lifetime shall be studied.
- To study the relative importance of the increased hydrodynamic load and additional non-structural mass.
- To compare the fatigue damage to the predictions from the simple model.

The NOWITECH 10 MW reference turbine is the basis of the study and the results can be published freely. The simulations are conducted in FEDEM Windpower, a simulation tool for dynamic analysis of complete wind turbine systems [7].

1.3 Structure of the report

The first part of Chapter 2 deals with the general background material needed to understand the analysis setup. Chapter 2 also introduces the topic of marine growth and its effects on a marine structures.

The effects are evaluated numerically for a simple beam at the start of Chapter 3. This chapter also includes a description of the analysis setup, including a convergence study to find the appropriate discretization level of the structure.

Chapter 4 presents and discusses the results from the analyses of the lattice tower structure. Stress variance spectra are presented for a number of reference points. The effect of marine growth on joint fatigue lifetime is presented.

Chapter 5 summarizes the results and gives conclusions and recommendations for further work.

Chapter 2

Theory

2.1 NOWITECH 10 MW reference wind turbine

2.1.1 General

The NOWITECH 10 MW reference turbine is a fictitious three-bladed, horizontal axis wind turbine with rated power 10 MW and main dimensions as depicted in Figure 2.1 [8]. The support structure is a four-legged, full-height lattice tower with a total height of 151 m. It is bottom fixed at 60 m water depth, the foundation consisting of a single driven steel-pile at each corner of the tower. The reference turbine is designed for a fictitious wind farm located offshore in the North Sea, characterized by strong winds, low wind shear and low turbulence. The environment is chosen to be relevant for the wind farms planned to be installed at Dogger Bank.

The wind turbine was developed in order to have a common wind turbine case for research purposes. Therefore, detailed descriptions of the blade aerodynamics and structural design, the Rotor Nacelle Assembly and control system are included. Research results can be published freely.

The wind turbine introduces the full-height lattice tower as support structure. The concept has been described by Long and Moe [9] and Muskulus [5]. Com-

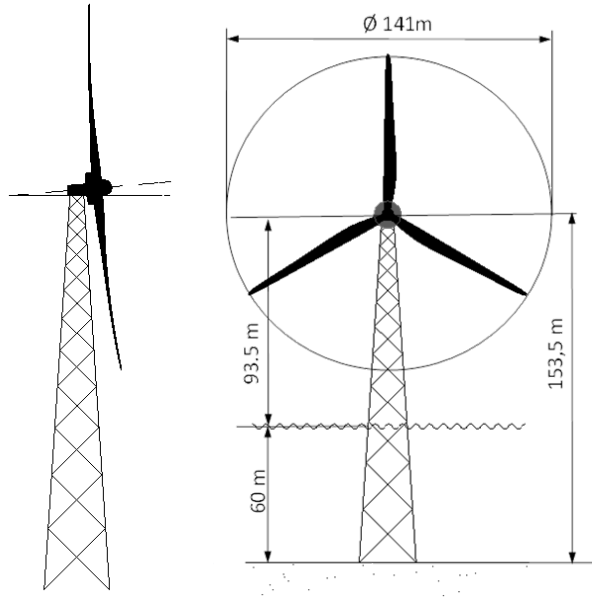

Figure 2.1: Main dimensions of the NOWITECH 10 MW reference turbine.

pared to the jacket structure concept, the advantage of the full-height lattice tower is that the expensive and fatigue-prone transition piece is removed. Also, significant savings in steel weight can be achieved. A draw-back is the complex fabrication. As the lattice tower concept introduces many welded joints, the production time increases.

2.1.2 Rotor characteristics

In front of any wind turbine tower, there is a retardation of the airflow. When the blades pass in front of the tower, the blades are less loaded and this results in a periodic impulse load. One blade passes the tower with a frequency given by the rotational speed of the rotor. By conventions, this frequency is called 1P. For a three-bladed wind turbine, excitations will occur with a fundamental frequency of 3P. A Fourier transform of the periodic impulse load reveals its higher harmonic components as 6P, 9P, 12P, etc.

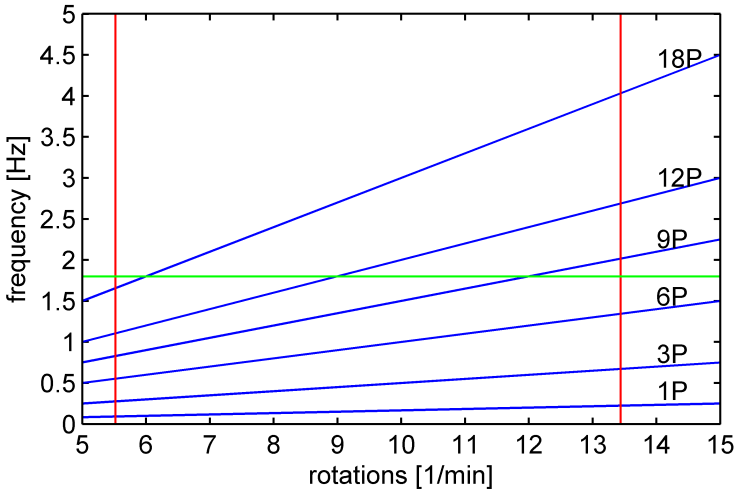

Figure 2.2: Campbell diagram for the NOWITECH 10 MW reference turbine.

The harmonic components can be plotted as function of rotor speed in a Campbell diagram, as shown in Figure 2.2. The turbine is working in the range between the cut-in and rated speed, indicated by red lines in the figure. The reference turbine has a cut-in speed of 5.54 rot/min and a rated speed of 13.44 rot/min. The natural frequencies of the support structure are (of course) independent of the rotor speed and can be plotted in the Campbell diagram for comparison. In Figure 2.2, the second natural frequency the tower, f =1.8 Hz, is plotted in green as an example. It is seen that within the working range of the rotor, resonance could occur between the this mode and the 9P, 12P and 18P-frequencies.

It is common to assume a linear relationship between the wind speed and the rotational speed of the rotor. If we also assume constant wind speed, the higher harmonics can be determined as precise values for a given wind speed. In reality, the instantaneous wind speed varies because of turbulence. Therefore, the rotor speed will vary in time and the higher harmonics accordingly. The widest possible range is given by using the cut-in speed and the rated speed as lower and upper bounds respectively. This approach gives very wide ranges for the nP-values. For a specific environmental condition, the range will be more limited.

2.2 Environmental conditions

In this section, an introduction to the environmental conditions responsible for loads on the support structure is given. The most important phenomena for offshore wind turbines are

- wind
- waves
- current

Other environmental aspects include tides, ice, earthquake, temperature variations and scour. For specific cases, these aspects may be important, but they are excluded from this report.

In general, natural phenomena vary in time and space in a random manner. Large amounts of experimental data are needed and the generalized, mathematical description must be able to describe the random process.

The description of the environmental conditions depend on the time scale. The conditions are assumed to be stationary for some short time interval. For waves, this interval typically varies between 20 minutes and 6 hours, whereas for wind it is typically 10 minutes. The short term, stationary environmental conditions are represented by a variance spectrum. Long term statistics deals with the long term distribution of the environmental parameters, such as the seasonal or yearly variations of the environmental conditions. A popular form of long term statistics is occurrence tables.

A short term representation of the environmental conditions has been used in the analyses. Therefore, descriptions of long term statistics are left out from this report.

2.2.1 Wind conditions

In this section, wind conditions will presented as described by DNV [10].

Wind data are height and time dependent. It is common to use 10 m height as a reference height and to assume stationary wind conditions over 10 minutes. Then, the wind conditions can be represented by the 10-minute mean wind speed U_{10} at height 10 m and the corresponding standard deviation σ_U of the

wind speed. In connection with wind turbines, the hub height may also be used as reference height.

The turbulence intensity is defined as the standard deviation of the wind speed divided by the mean wind speed, as represented by the following ratio

$$I_t = \frac{\sigma_U}{U_{10}} \tag{2.1}$$

Wind profile

The wind profile denotes the mean wind speed as a function of height above ground or sea surface. Several wind profiles are available, the following is a power law wind profile:

$$U(z) = U(z_{ref}) \left(\frac{z}{z_{ref}} \right)^{\alpha} \tag{2.2}$$

where z is the height above the ground or sea surface. The power law exponent α depends on the terrain in consideration. IEC [11] recommends $\alpha = 0.14$ for offshore locations.

Wind spectrum

The short term, stationary wind conditions are characterized by a wind spectrum. The following Kaimal wind spectrum is one of several available wind spectra. This spectrum will be used when describing the wind conditions in the analyses.

$$S_U(f) = \sigma_U^2 \frac{6.868 \frac{L_u}{U_{10}}}{\left(1 + 10.32 \frac{f L_u}{U_{10}}\right)^{5/3}} \tag{2.3}$$

where f denotes frequency and L_u is an integral length scale that may be taken as

$$L_u = 3.33\,z \quad \text{for } z < 60 \text{ m}$$
$$L_u = 200 \text{ m} \quad \text{for } z \geq 60 \text{ m}$$

where z is the height above the ground or sea water level.

2.2.2 Wave conditions

Ocean waves are irregular and random in amplitude, length and speed of propagation. Therefore, a stochastic wave model is needed to describe the sea state. The sea state is represented as a superposition of individual regular waves that have a specified wave height, frequency and phase angle [12]. In this section, a short review of the theory of such linear waves is given, before it is explained how irregular sea states can be described.

Regular waves

Regular wave theory assumes a horizontal sea bottom and a horizontal free surface. The governing equations are derived from potential flow theory, assuming the sea water to be an incompressible and irrotational fluid [12].

The instantaneous wave elevation $\eta(x,t)$ for a regular wave propagating in the positive x-direction is given as

$$\eta(x,t) = a\sin(\omega t - kx) \tag{2.4}$$

where a is the wave amplitude, one half of the wave height H. The angular frequency ω and the wave number k are given as

$$\omega = \frac{2\pi}{T} \tag{2.5}$$

$$k = \frac{2\pi}{\lambda} \tag{2.6}$$

where T is the wave period and λ is the wave length.

The relationship between the wave number k and the angular frequency ω is given by the dispersion relation

$$\omega^2 = gk \tanh kd \tag{2.7}$$

where g is the acceleration of gravity and d is the water depth. The interpretation of the dispersion relation is that for a given frequency, the wave length is uniquely determined. Thus, to describe a wave, the wave height and the frequency must be specified.

The velocity u and acceleration $\dot{u}$ of a water particle in the x-direction is given below. Also, the velocity w and acceleration $\dot{w}$ in the z-direction, the depth-direction, is given.

$$u = \omega a \frac{\cosh k(z+d)}{\sinh kd} \sin(\omega t - kx) \tag{2.8}$$

$$w = \omega a \frac{\sinh k(z+d)}{\sinh kd} \cos(\omega t - kx) \tag{2.9}$$

$$\dot{u} = \omega^2 a \frac{\cosh k(z+d)}{\sinh kd} \cos(\omega t - kx) \tag{2.10}$$

$$\dot{w} = -\omega^2 a \frac{\sinh k(z+d)}{\sinh kd} \sin(\omega t - kx) \tag{2.11}$$

Irregular waves

The wave elevation of an irregular sea can be represented as the sum of a large number of regular wave components [12]. Each component is assigned a specified amplitude a_j, frequency ω_j, wave number k_j and a random phase angle ϵ_j

$$\eta = \sum_{j=1}^{N} a_j \sin(\omega_j t - k_j x + \epsilon_j) \tag{2.12}$$

The wave amplitudes can be found from a wave spectrum using the following relation

$$\frac{1}{2}a_j^2 = S(\omega)\Delta\omega \tag{2.13}$$

When the wave amplitude have been found, the water particle velocity and acceleration can be determined by Equations (2.8) - (2.11).

Wave spectra

Two common wave spectra are the Pierson-Moskowitz spectrum and the JONSWAP spectrum. The two spectra are plotted in Figure 2.3. Both spectra are characterized by the significant wave heigth H_S and the peak wave period T_p.

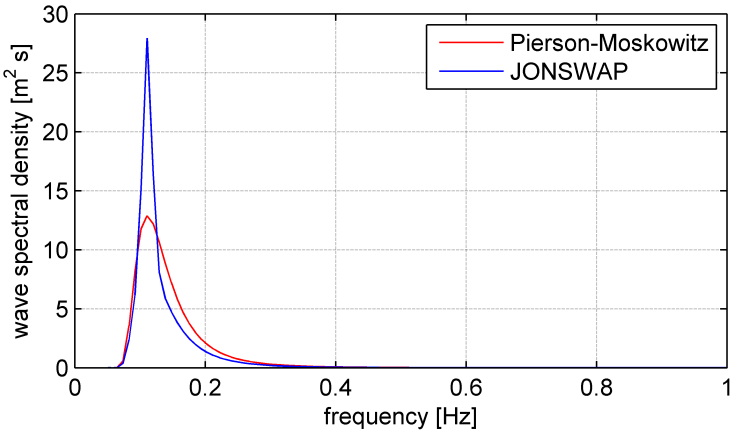

Figure 2.3: Pierson-Moskowitz and JONSWAP wave spectra.

The Pierson-Moskowitz spectrum [13] $S_{PM}(\omega)$ describes a fully developed sea with infinite fetch.

$$S_{PM}(\omega) = \frac{5}{16}\, H_S^2\, \omega_p^4\, \omega^{-5}\, exp\left[\frac{5}{4}\left(\frac{\omega}{\omega_p}\right)^4\right] \tag{2.14}$$

The JONSWAP spectrum $S_J(\omega)$ is formulated as a modification of the Pierson-Moskowitz spectrum. It was developed based on data from the Joint North Sea Wave Observation Project (JONSWAP) in 1973 [14].

$$S_J(\omega) = A_\gamma \, S_{PM}(\omega) \, \gamma^{exp\left(-0.5\left(\frac{\omega-\omega_p}{\sigma\omega_p}\right)^2\right)} \tag{2.15}$$

where γ is a peak shape parameter, σ is a spectral width parameter and A_γ is a normalizing factor

$\sigma = \sigma_a$ for $\omega \leq \omega_p$
$\sigma = \sigma_b$ for $\omega \geq \omega_p$
$A_\gamma = 1 - 2.87 \ln(\gamma)$

Typical numerical values are given by DNV [10]: $\gamma = 3.3$, $\sigma_a = 0.07$ and $\sigma_b = 0.09$.

The JONSWAP spectrum may be used for developing sea states with limited fetch. The shape is characterized by a narrower peak than the Pierson-Moskowitz spectrum. When γ is set to unity, the JONSWAP spectrum reduces to the Pierson-Moskowitz spectrum. The JONSWAP spectrum is expected to be a reasonable model when [10]

$$3.6 < \frac{T_p}{\sqrt{H_S}} < 5 \tag{2.16}$$

2.3 Environmental loads

In this section, it will be explained how the environmental loads on the wind turbine can be calculated.

2.3.1 Wind loads

The calculations of the aerodynamic loads were done by software packages. Only a very brief introduction to the used method is given here.

To calculate the loads on the turbine, blade-element and momentum theory is used. The turbine acts as an actuator disk by slowing the airflow, creating a wake with reduced airflow velocity. To achieve this, the actuator disk exerts a force on the flow.

To estimate this force, each blade is divided into a finite number of blade elements, each with specified aerodynamic features. The aerodynamic coefficient is introduced to account for the shape and the surface roughness of the blade element. Then, the force on the element depends on the aerodynamic coefficient, the projected area and the wind velocity and angle of attack. Both drag and lift forces are calculated. The forces are then summed up along the blade axis and over one rotor revolution in order to obtain the forces and moments produced by the entire rotor.

2.3.2 Hydrodynamic loads

Morison's formula

A structure placed in a wave field will experience a time-dependent force from the water flow. For our purpose, the force on slender cylinders is of interest. The wave forces can be calculated by Morison's formula as long as the cylinder does not modify the incident wave field significantly. According to DNV [10], this criterion is satisfied when

$$\lambda > 5D \tag{2.17}$$

where λ is the wave length and D is the cylinder diameter. Morison's formula states that the in-line force per unit length of the cylinder may be expressed as

$$dF = \frac{\rho}{2} C_d D \, u|u| + \rho \, C_m \, \frac{\pi}{4} D^2 \, \dot{u} \tag{2.18}$$

where ρ is the water density and D is the cylinder diameter. C_d and C_m represent the dimensionless drag and inertia coefficient respectively, $u = u(t)$ and $\dot{u} = \dot{u}(t)$ represent the undisturbed water velocity and acceleration.

The force comprises of two terms; the drag term, proportional to the square of the fluid velocity and the inertia term, proportional to the acceleration of the fluid.

$$\begin{aligned} f_D &= \frac{\rho}{2} C_d D \, u|u| \qquad \text{drag term} \\ f_I &= \rho \, C_m \, \frac{\pi}{4} D^2 \, \dot{u} \quad \text{inertia term} \end{aligned} \tag{2.19}$$

Since u^2 and $\dot{u}$ reach their maximum value at different points in time, the two terms will be out of phase. The relative importance of the terms is governed by the ratio of the wave height to the member diameter. The relation between the maximum values can be written as [10]

$$\frac{f_{D,max}}{f_{I,max}} = \frac{1}{\pi}\frac{C_d}{C_m}\frac{H}{D} \tag{2.20}$$

As seen from Equation (2.20), the inertia term dominates for large member diameters D and/or small wave heights H.

To find the total force on the cylinder, the load contributions are integrated along the cylinder axis

$$F = \int_L dF \tag{2.21}$$

Forces on inclined members For inclined members the incoming flow will not be normal to the member length axis. In this report, the *cross flow principle* is assumed to hold. Then, the normal force on the inclined cylinder can be calculated simply by taking only the normal component of the water particle velocity.

The tangential drag force is mainly caused by skin friction and is small compared to the normal drag force. It may be important for long, slender elements with a considerable tangential velocity component. In this report, the tangential drag force is neglected.

The effect of sea current For combined wave and current flow conditions, the water particle velocities caused by the waves and current should be added as vector quantities. Then, the drag force on the cylinder can be calculated as described above.

Hydrodynamic coefficients The drag and inertia coefficients C_d and C_m need to be found experimentally. In general, they depend on the Reynolds number Re, the Keulegan-Carpenter number K_C and the surface roughness of the cylinder

$$Re = \frac{uD}{\nu} \tag{2.22}$$

$$K_C = \frac{\pi H}{D} \tag{2.23}$$

where ν is the kinematic viscosity of the fluid, H is the wave height and D is the cylinder diameter.

The influence of these parameters on the hydrodynamic coefficients is described in detail in the standards by DNV [10], ISO [15] and NORSOK [16]. In general, they agree and they also give further references. The following is based on DNV [10].

In the so-called post-critical regime, characterized by high Reynolds numbers and high K_C-numbers, the following asymptotic values for drag coefficients can be used.

$C_d = 0.65$	smooth cylinder
$C_d = 1.05$	rough cylinder

A post-critical regime can normally be assumed in the extreme design environment. However, for the fatigue design environment, the Reynolds number may drop to a critical flow regime, at least for smooth cylinders. For rough cylinders, a post-critical regime can be assumed also in the fatigue limit state.

For small K_C numbers, special considerations are necessary. For smooth cylinders, the drag coefficient may attain values in the range $C_d = 0.20$ – 0.85. For rough cylinders the range is $C_d = 0.52$ – 1.52.

The value of the added mass coefficient C_m depends on K_C as shown in Figure 2.4. The asymptotic values for large K_C-values are

$C_m = 1.6$	smooth cylinder
$C_m = 1.2$	rough cylinder

Vortex shedding and lift forces

So far, the in-line forces resulting from the flow passing a cylinder have been considered. Depending on the flow characteristics, vortices may form in the wake

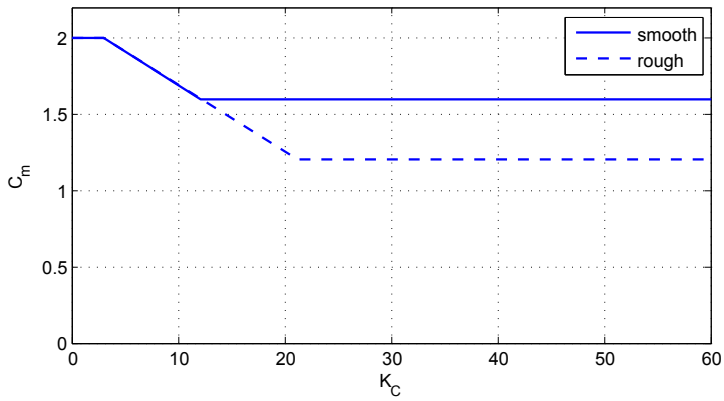

Figure 2.4: Inertia coefficient C_m as a function of K_C-number

behind the cylinder. The term *vortex shedding* is used for the phenomenon that the vortices are torn away from the cylinder, causing so-called lift forces in the transversal direction. The Strouhal number S_t is used to characterize vortex shedding.

$$S_t = \frac{f\,D}{u} \tag{2.24}$$

where f is the vortex shedding frequency, the number of vortex pairs per second. D is the cylinder diameter and u is the incident flow velocity.

When vortex shedding occurs, the Strouhal number typically has the value $S_t = 0.2$.

2.4 Material fatigue

Material fatigue is the term used for progressive, localized structural damage that is caused by cyclic loading. It is related to the growth of microscopic cracks in the material. Such cracks will always be present in welded structures. When the crack reaches a critical size, the structure will suddenly fracture.

Because the lattice tower is a welded structure subjected to cyclic loads from the wind and the waves, fatigue considerations are important for the design [17].

2.4.1 S–N-curves

The fatigue life N_{max} is the number of stress cycles at a particular magnitude that a component can withstand before fatigue failure. The dependence on the fatigue life on the stress range is presented graphically in an S–N-curve. An example of an S–N-curve is given in Figure 2.6.

The equation for the S–N-curve is

$$\log N_{max} = \log \overline{a} - m \log \Delta\sigma \tag{2.25}$$

where m is the negative inverse slope of the S–N-curve and $\log \overline{a}$ is the intercept of the $\log N_{max}$-axis by the S–N-curve.

Design standards like those of DNV [1] and Eurocode [18] include a number of S-N-curves for various structural details. A point on the S–N-curve is found by testing a specific detail undergoing sinusoidal stress variations, recording the numbers of cycles required to fail the component. By testing similar specimens at different stress ranges, the S–N-curve is created. Typically, S–N-curves for low-carbon steels have a branch with a slope $m = 3$ for the lower cycles and a branch with slope $m = 5$ for the higher cycles. For welded specimens, the mean stress does not influence the fatigue life significantly; only the stress variation needs to be considered.

2.4.2 Rainflow counting

The stress in a real component will vary in a more complex manner than a simple sinusoidal function. From a spectrum of varying stress, we need to find an equivalent number of stress cycles. The rainflow counting algorithm is a commonly used method for this purpose [19]. The method received its name because its graphical representation resembles rain running off a pagoda roof, as shown in Figure 2.5. The result from the rainflow counting is a set of values for $N(\Delta\sigma_i)$, the equivalent number of cycles within the specified stress range $\Delta\sigma_i$.

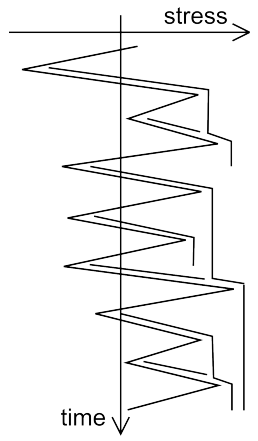

Figure 2.5: Illustration of the rainflow counting algorithm.

2.4.3 Palmer-Miner summation rule

When the rainflow counting has been performed,values for $N_{max}(\Delta\sigma_i)$, can be found from the S–N-curve. Then, the total fatigue damage D can be found using the Palmer-Miner rule summation rule:

$$D = \sum_i \frac{N(\Delta\sigma_i)}{N_{max}(\Delta\sigma_i)} \tag{2.26}$$

The Miner rule states that the detail will not fail due to fatigue as long as $D \leq 1$

2.4.4 Fatigue design of tubular members

The weld at the intersection between two or more tubular members must be designed for fatigue. The hot spot stress should be evaluated at eight spots around the circumference of the intersection to combine the axial stress, and the stress from in-plane and out-of-plane bending. Stress concentration factors are given by DNV [1]. The S–N-curve for tubular joints in seawater with cathodic protection is given in Figure 2.6.

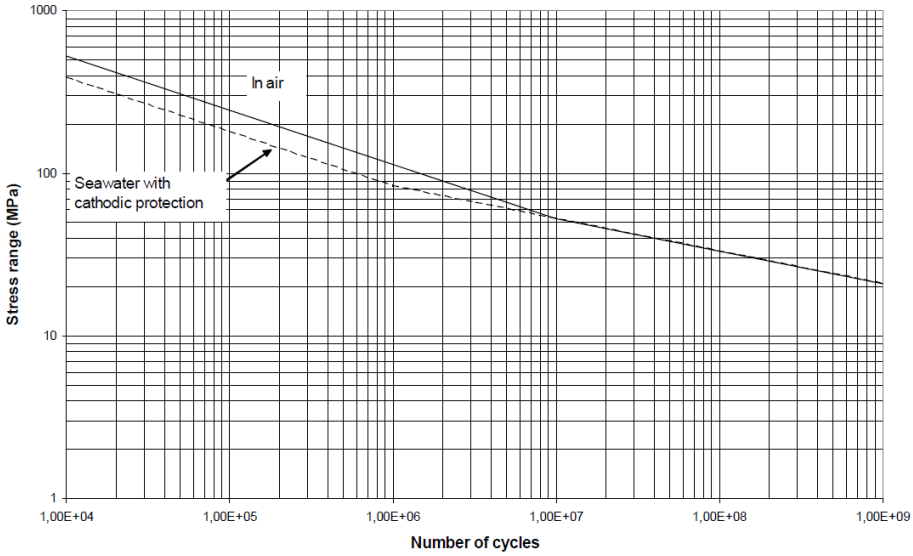

Figure 2.6: S–N-curve for tubular members [1].

2.5 Marine growth

2.5.1 General

Biofouling is the unwanted settlement and growth of marine organisms, including micro-organisms, algae and animals, on underwater surfaces of ships, buoys, piers, offshore platforms, industry heat exchange equipment etc [20]. Other terms for the same phenomenon include marine growth and marine fouling.

The biological composition of the growth varies with the biogeographical region. In this report, the focus will lie on the North Sea and water depths less than 100 m.

Using the terminology of Oldfield (ed.) [2], marine growth is subdivided into the following categories:

Mussels
: Frequently dominant. Hard exterior, firmly attached.

Kelp
Long frond-like growths.

Algae (other than kelp)
Soft, branching.

Barnacles, tubeworms, limpets etc.
Hard, firmly attached growth; mostly one organism thick; difficult to remove.

Hydroids, bryozoa
Soft, branching and compressible growths.

Sponges, anemones, sea-squirts, alcyonium
Soft bodied, often bulky organisms.

2.5.2 Biology

Many factors influence on the amount and type of marine growth. These factors include physical factors such as temperature, salinity, water depth and wave action, as well as biological factors such as predators, larval supply, nutrient and food availability, biology and physiology of the individual species. Some of these factors depend on each other. For instance will salinity, temperature, food resources and sun light penetration all change with depth [21].

Biological studies have been conducted on several oil and gas platforms in the North Sea [2,21–24]. The platforms are typically placed on soft, muddy bottom, forming artificial reefs for species that require hard substrata. The studies show that some organisms typically dominate in specific depths and that in general, marine growth thickness and biomass decreases with depth. The recruitment and colonization of the structure is a highly dynamic process. Whomersley found that even 11 years after installation, the fouling communities were still changing [22].

The dominant species found on North Sea platforms include *Mytilus edulis* (blue mussel), *Tubularia larynx* (hydroid), *Metridium senile* (anemone), *Alcyonium digitatum* (soft coral), *Filograna implexa* (tubeworm), *Balanus hameri* (barnacle), *Ascidiella scabra* (sea squirt) and bryozoans [21–24].

Blue mussels deserve our special attention because they dominate the upper 20 to 30 m of the structure where they are found. However, they are typically

shoreline or shallow-water animals, usually not found in deep water. To colonize an offshore platform, they must be transported as planctonic larvae out to the platform by oceanic currents. This must happen before they metamorphose, a process lasting two to three weeks at North Sea temperatures.

To clarify how important the oceanic currents are for this specie, the fouling characteristics for two petroleum fields will be described. The Forties Field platforms are situated about 110 miles, far off from the coast, but surprisingly, mussels are common here. This is caused by the well defined currents sweeping the Scottish coast before continuing out past these platforms. Larvae are picked up by the current and transported to the Forties field. The Montrose field is situated less than 30 miles to the south of Forties, but it lies in the central North Sea water and is not influenced by the coastal current. Hence, there are very few mussels on the Montrose platform. [23, 24].

Below the mussel zone, the primary colonizers are tubeworms and hydroids. Eventually, secondary colonizers, including anemones and soft corals will become the dominant organisms. They will out-compete the hydroids and tubeworms by competition over the nutrient supply and overgrowing them [22] and may become the dominant species after 3-8 years, depending on region.

2.5.3 Marine growth levels

Using the terminology of Oldfield (ed.) [2], the North Sea is divided into three regions. The term *southern region* refers to the North Sea south of latitude 56°N, *central region* to the region bounded by 56°N and 58°N, and *northern region* to areas north of 58°N.

In the *southern region*, extensive marine growth is reported. After installation, the marine growth quickly reaches a well established level. Mussels dominate in depths less than 30 m; hydroids, tubeworms and barnacles are common at greater depths. Algae are found in the top 10 m. The two main reasons for the extensive growth in this region are the proximity to the coast and the near-shore currents that sweep the area.

In the *central region*, the predicted levels of marine growth are more uncertain as the observed levels differ from platform to platform. In this area, several oceanic currents meet and the current system is complex. In general, mussel fouling is sparse. At the platforms where it is more pronounced, growth rates are never as rapid as in the southern fields.

The *northern North Sea* is not considered relevant for this thesis, because of the water depth and the long distance to shore.

Table 2.1 gives a forecast on predicted growth thicknesses for the southern and central regions of the North Sea, taken from Oldfield (ed.) [2]. The numbers are based on thicknesses reported by 12 platforms operators. The thickness values are to be used together with the depth profiles in Figure 2.7.

Oldfield (ed.) [2] also gives a map, indicating the approximate limit of heavy mussel fouling in the waters around the UK. The map reproduced in Figure 2.8.

Table 2.1: Predicted biofouling thicknesses in regions of the North Sea.

	Indicative thickness of fouling [mm]							
	Mussels				Hydroids, bryozoa			
	After				After			
	1-2	3-4	7-8	12-15	1-2	3-4	7-8	12-15
Region of the North Sea	years in water				years in water			
Southern	80	150	200	200	30	50	60	60
Central, upper bound	60	70	150	150	-	90	110	110
Central, lower bound	-	30	80	80	-	60	60	60

2.5.4 Removal of marine growth

Prevention of biofouling on ship's hulls plays an important role in reducing fuel consumption and several strategies have been adapted to manage marine growth on ship's hulls. Typically, fouling control coatings are used. Biocide-free coatings provide a smooth, low-friction surface that the fouling organisms have difficulties attaching to. Biocide containing antifoulings release biocides at a controlled rate and these coatings may yield up to 90 months of fouling control.

Marine growth is regularly removed from jacket oil and gas platforms also for reasons other than that of structural loading. Marine growth is associated with pitting corrosion, due to so-called sulfate-reducing bacteria that thrive in the oxygen-poor micro-habitats beneath both hard and soft marine growth [23,25]. Also, marine growth may conceal cracks and corroded surfaces and must be removed prior to visual inspection and maintenance by divers or remotely operated vehicles [21].

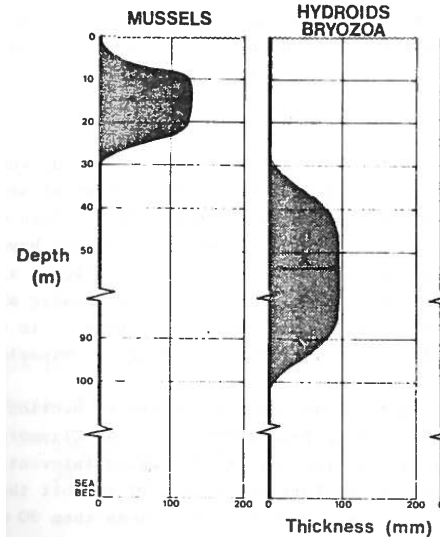

Figure 2.7: Depth profiles to be used together with Table 2.1. Taken from Oldfield (ed.) [2].

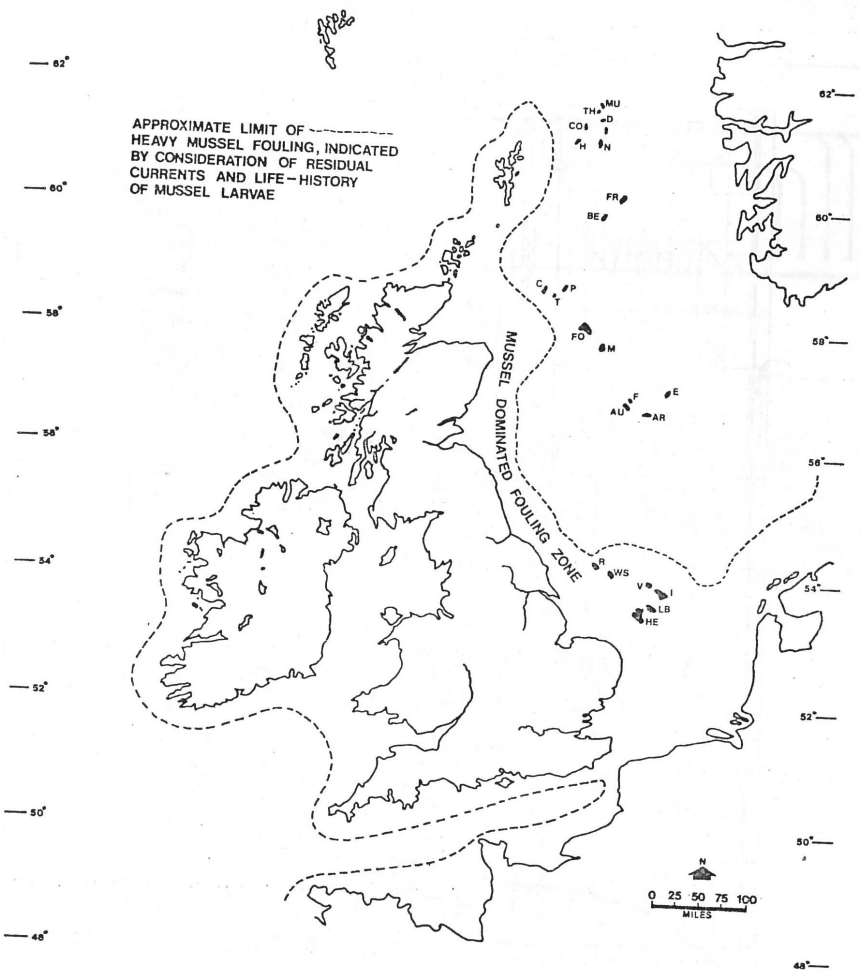

Figure 2.8: Indicative limit of heavy mussel fouling in UK waters. Taken from Oldfield (ed.) [2].

The use of coatings requires that the structure regularly is moved to a dry dock in order to apply new layers. An alternative for bottom-fixed structures is to physically remove the growth on-site by high pressure water jetting. This is a costly procedure, as it has to be performed by divers.

Another option is to use so-called wave driven marine growth preventers. This apparatus consists of a number of rings moving up and down along the jacket members, preventing organisms from attaching. It may also be used for removal [26].

2.5.5 Recommendations given in standards

The ISO 19901 standard [27] gives some general considerations on marine growth. The influence of marine growth on hydrodynamic actions originates from increased mass and increased drag force. Both the location, the age of the structure and the maintenance regime influence on the type and the amount of marine growth. Because the marine growth is site-specific, experience in one part of the world cannot necessarily be applied to another.

Circular cross- sections are classified as smooth or rough and structural elements may only be considered smooth if they are located above the highest astronomical tide or sufficiently deep that the marine growth is sparse enough to ignore its effect on roughness.

According to the ISO 19902 standard [15], the mass of marine growth that is expected to accumulate on the structure shall be included in the dynamic model of a fixed structure. Typical values for hydrodynamic coefficients for the rough and the smooth case are given.

The NORSOK standard [3] prescribes values for the thickness of marine growth that may be used if no more detailed values are available. The values are reproduced in Table 2.2. The standard also says that the thickness of the marine growth is assumed to increase linearly to the given value over the first two years after installation. The mass density of marine growth in air may be set equal to $\rho_{MG} = 13$ kN/m^3.

Table 2.2: Marine growth thickness recommended by NORSOK for latitudes 56°N to 59°N [3].

Water depth [m]	MGT [mm]
Above +2	0
+2 to -40	100
Below -40	50

2.6 Effects of marine growth on a structure

2.6.1 Increase in structural weight

As marine growth has a higher specific gravity than seawater, marine growth will potentially increase the dead load on marine structures. For fictitious, but representative oil and gas platforms, this effect has been shown to be negligible [28, 29]. The weight of marine growth was insignificant compared to the total weight of the structure.

When compared to oil and gas platforms, both the dead load and the structural weight of a wind turbine substructure will be much smaller. Still, we expect that the weight of marine growth will only constitute a small part of the total weight.

2.6.2 Alteration of the natural frequencies

The natural frequency for a single degree of freedom system is given as [30]

$$\omega_e = \sqrt{k/m} \tag{2.27}$$

where k represents the system stiffness and m represents the system mass.

Marine growth will not contribute to the structure stiffness, but represents an increase in the total mass. Thus, marine growth will potentially lower the natural frequency. Multiple degree of freedom systems, like the lattice tower structure, will have many natural frequencies. Then, the effect will basically be the same, but some natural frequencies may be more sensitive to changes in marine growth than other.

2.6.3 Increase in wave loading

Increase in diameter

For convenience, Morison's formula is repeated:

$$dF = \frac{\rho}{2g} C_d D\, u|u| + \frac{\rho}{g} C_m \frac{\pi}{4} D^2 \dot{u} \tag{2.28}$$

Marine growth represents a increase in the diameter D and the drag loads on the cylinder will increase. From Equation (2.28), it can be expected that the force on the cylinder increases linearly with D if the drag term dominates and with D to the second power if the inertia term dominates.

Increase in surface roughness

Marine growth also increases the surface roughness. Already a small amount of growth will change the surface to perfectly smooth to a coarser surface. A thicker layer of marine growth may increase the surface roughness further, but this is more difficult to quantify. Surface roughness must be taken into account already with small marine growth thickness.

According to DNV [10], the hydrodynamic coefficients for rough cylinders may be considered independent of Reynolds number both for extreme design environment as well as for the fatigue calculations. Then, the hydrodynamic coefficients may be taken as $C_d = 1.05$ and $C_m = 1.2$. For smooth cylinders, the corresponding values would be $C_d = 0.65$ and $C_m = 1.6$. A small increase in surface roughness from perfectly smooth to a small roughness will alter the C_d and C_m-values significantly.

The drag force calculated by in Equation (2.28) is normally dominated by one of the terms.Then, only the increase in the dominating term has an effect. A change in C_m is less important when the drag term dominates, and vice versa. The inertia coefficient C_m decreases for a rough cylinder. However, this is only valid for high K_C-numbers, when the drag term of Morison's equation is dominating.

2.6.4 Increase in flow instability

The effect of marine growth on vortex shedding is not straightforward. Marine growth increases the the member diameter in the expression for the Strouhal number, Equation (2.24). Wolfram showed that this will increase the strength of the vortices and their spanwise coherence, increasing the cyclic lift forces [[31], cited from [28]]. Also, an intermediately roughened cylinder has been shown to shed vortices regularly at Reynolds numbers where smooth cylinders showed only weak shedding [[32], cited from [29]].

On the other hand, it has been suggested that the presence of long, flapping kelp may reduce vortex shedding. However, this has not been verified by experiment, as least not as known to the author. On the contrary, Nath investigated the flow characteristics around heavily roughened cylinders and vortex shedding was always present, even for very long kelp-like covering [33]. Heaf concludes that the presence of marine growth is unlikely to mitigate the effect of vortex shedding in waves [29].

Vortex shedding will not be studied any further in this report.

Chapter 3

Methods

3.1 Exercise: Numerical study of a simple beam

In this section, the effects of marine growth as described in Section 2.6 will be evaluated numerically. The objective is to try and predict the effect the marine growth will have on the lattice tower.

Several simplified models will be used as appropriate. The vertical beam described in Section 3.1.1 is thought to represent a single member of the lattice structure. In Section 3.1.3, the entire lattice tower will be simplified as a cantilever beam.

3.1.1 The simple beam model

The beam depicted in Figure 3.1 has a length L and is clamped at both ends. The outer diameter D and the wall thickness T determine the beam mass m as well as the area moment of inertia I. The added mass resulting from the marine growth layer with thickness T_{MG} is denoted m_{MG}.

The member length L, outer diameter D and wall thickness T vary over the lattice tower. In Table 3.1, representative geometric properties for members below the water line are given. These values will be used when the effects of marine growth are evaluated.

The simple beam is thought to represent a vertical member of the lattice structure. However, if the beam is a part of the structure, there will be some rotational stiffness at the support, but it will not be totally clamped. Thus, the simplification with clamped ends makes the simple beam too stiff.

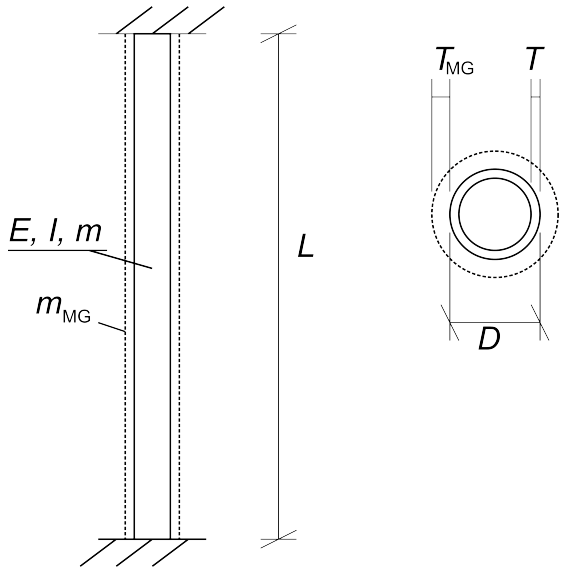

Figure 3.1: Geometry of the simple beam.

Table 3.1: Representative geometric properties of brace and leg members.

	L [m]	D [m]	T [m]
Leg members	20	0.70 – 1.00	0.04 – 0.05
Brace members	30	0.45 – 0.85	0.03 – 0.05

3.1.2 Increase in structural weight

To give an estimate of the weight of the marine growth, compared to the structural weight, calculations similar to those of Heaf [29] have been performed. Marine growth was applied to all members down to a depth of 30 m. The

resulting submerged weight of the marine growth is given in Table 3.2. The total structural weight was assumed to be 1520 tonnes and the mass density of the marine growth was set to ρ_{MG} 1300 kg/m^3. Compared to the estimate by Heaf [29], the ratio of the weight of marine growth to the total weight is of order ten higher.

Table 3.2: Submerged weight of marine growth.

MGT [m]	Mass of MG [kg]	Mass of MG to total structural weight [%]
0,05	10731	0.7
0,10	23150	1.5
0,15	37257	2.5
0,20	53053	3.5

3.1.3 Alteration of the natural frequencies

When the effect of marine growth on the natural frequencies shall be predicted, it is convenient to distinguish between the global modes, where the the lattice tower deforms as one part, and local modes, which also include some out-of-plane deformation of the bracing [34].

To estimate the change of the first natural frequency, corresponding to the "fore-aft" mode, a cantilever beam representing the whole tower is suggested. Using Euler-Bernoulli beam theory, it may be shown that the first natural frequency of a cantilever beam is given by

$$\omega_e = 1.875^2 \sqrt{\frac{k}{m}} \tag{3.1}$$

where k represents the beam stiffness and m is the total mass. Marine growth will not contribute to the structure stiffness, but increase the total mass by a contribution m_{MG}. Hence, the change of the first natural frequency with marine growth can be written

$$\frac{\omega_{MG} - \omega}{\omega} = \sqrt{\frac{m}{m + m_{MG}}} - 1 \tag{3.2}$$

This equation has been evaluated using the values for mass of marine growth to total structural mass from Table 3.2. The predictions, given in Table 3.3, show show that only small changes in global natural frequencies can be expected. For a maximum marine growth thickness of 0.20 m, only 2% change for the global natural frequencies is expected.

In these calculations, it has been assumed that the marine growth is uniformly distributed along the lattice tower. In reality, the marine growth is placed close to the clamped end such that the effect will be even less than predicted in Table 3.3. Assuming that the lattice tower is equally stiff along its length axis is another simplification.

Table 3.3: Change in first natural frequency for cantilever beam.

MGT [m]	Mass of MG to total structural mass [%]	Change in natural frequency [%]
0.05	0.7	-0.3
0.10	1.5	-0.8
0.15	2.5	-1.2
0.20	3.5	-1.7

In a local mode shape, the braces will deform out of the side plane of the lattice tower. Hence, the stiffness of the brace members and not the leg members is of interest. The simple beam of Section 3.1.1 is used as basis and the first natural frequency is given by

$$\omega_e = 4.7^2 \sqrt{\frac{EI}{(m + m_{MG})\, L^3}} \tag{3.3}$$

The formula has been evaluated for the brace member geometries in Table 3.1. The effect on the beam natural frequency is given in Table 3.4, which summarizes the calculations done in Appendix A.

The initial natural frequency is smaller for the more slender brace members. For these members, the relative change in natural frequency is larger.

As noted in Section 3.1.1, the assumption with clamped ends makes the beam too stiff. Therefore, the local mode natural frequencies of the lattice tower will

have lower values than the values given in Table 3.1. However, the relative change could be expected to be within the same range. Because the members are quite similar, the result from many members should be the same as for one.

Table 3.4: Change in natural frequency for the simple beam.

MGT [m]	Natural frequency [Hz]	Change in natural frequency [%]
0	8.5 – 16	
0.1		-15 – -24
0.2		-27 – -40

3.1.4 Increase in wave loading

Increase in diameter

From Section 2.6.3, it can be expected that the force on the cylinder increases linearly with D if the drag term dominates and with D to the second power if the inertia term dominates. In Figure 3.2, the inertia term in Morison's formula is plotted for three representative member diameters. The increase in the inertia term is plotted for increasing diameter due to marine growth, maximum 0.20 m. For each member, the wave height was chosen such that $f_{I,max} = 2\, f_{D,max}$, implying that the inertia term is dominating. It is seen that the effect of the diameter D to the second power is very small; the increase in the inertia term is effectively linear. It is concluded that within the relevant diameter range, the increase in drag force calculated from Morison's formula is in effect linear with respect to D, independent of which term dominates.

The relative change in drag load for the member geometries in Table 3.1 are given in Table 3.5. The calculations were done with sinusiodal waves and a wave height $H = 4$ m. This corresponds to the significant wave height used for the full analyses, $H_S = 4$ m. The peak wave period was then $T_p =$ 9 s. Here, the the load are evaluated for periods $T = 7$ s, $T = 9$ s and $T = 12$ s. The complete calculations are given in Appendix A.

In Table 3.5, the lower values correspond to initially high loads, that is, for small periods T, given the constant wave height H. For larger periods T, the initial load in the structure is smaller and the increase in drag force F_D is larger.

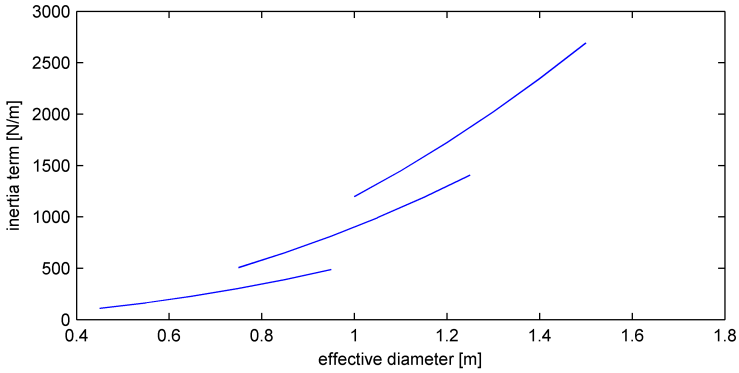

Figure 3.2: Inertia term of Morison's formula for representative diameters.

As seen in the table, the increase in drag load is large, both for brace and leg members.

Table 3.5: Change in drag load according to Morison's formula.

	MGT [m]	Relative change in dF_D [%]
Leg members	0.10	40.2 - 50.2
	0.20	90.5 -116.7
Brace members	0.10	43.6 - 64.2
	0.20	99.9 - 149.9

Increase in surface roughness

In Section 2.6.3, it was pointed out that the hydrodynamic coefficients will change when the surface changes to smooth to rough. However, this must be accounted for with just a thin layer of marine growth.

In this report, the effect of the hydrodynamic coefficients will not be explored any further. In the simulations, the coefficients are taken as $C_d = 1.00$ and $C_m = 2.0$.

3.1.5 Conclusions and predictions

Only small changes in global–mode natural frequencies can be expected. For a marine growth thickness of 0.20 m, less than 2 % change for the first natural frequencies is expected. The local–mode natural frequencies are expected to be more sensitive to marine growth. Predictions on the changes are given in Table 3.4. For a marine growth thickness of 0.10 m, up to 24 % decrease is predicted; for 0.20 m thickness, up to 40 % decrease.

From Morison's formula, the wave loads could be expected to increase by the diameter to the second power when in the inertia term dominates. However, for the diameter range in consideration, the increase is effectively linear, independent of which term dominates.

Due to the small initial diameter, the increase in wave loading is large. For a marine growth thickness of 0.10m, up to 64 % increase is predicted; for 0.20 m thickness, up to 150 %. The effect of the increased wave loading on the lifetime of the lattice tower, also depends on the relative importance of the wave loads, the wind loads and the harmonic loads from the wind turbine.

The hydrodynamic coefficients change significantly when the surface roughness changes from smooth to rough. However, this effect will not be explored any further.

3.2 Modelling the structure

3.2.1 Analysis setup

The analyses have been conducted using a code by Daniel Zwick, PhD student at NTNU. The code was made for an optimization process of the lattice tower [35]. The first step is a simulation of the lattice tower in Fedem Windpower, as described in the subsequent sections. The result is time series of forces and moments for each member and joint, which the code utilizes to analyse the tower for the ultimate limit state and fatigue limit state. The analysis includes calculation of stress concentration factors to determine the hot spot stresses in the joints. The code has been modified to include marine growth.

3.2.2 Simulation in Fedem Windpower

Fedem Windpower is a multibody dynamics finite element tool. Using this program, a finite element model of the wind turbine structure, the wind loads and hydrodynamic loads, as well as the control system are integrated in one solver.

The simulations were conducted in the time domain and the total simulation time was 180 s. When the simulation starts, the wind turbine has an initial rotational speed, but this speed does not necessarily correspond to the wind speed. Therefore, the results from the start-up phase will be misleading. To compensate for this, the results from the first 60 s are discarded before any further postprocessing.

The integration algorithm was Newmark integration with numerical damping.

3.2.3 State of the environment

The wind environment was described by a power law profile with mean wind speed at hub height $U_{hub} = 13.0$ m/s, turbulence intensity $I_t = 16$ % and power law exponent $\alpha = 0.14$. A Kaimal wind spectrum was used.

The wave environment was an irregular sea state described by the JONSWAP spectrum. The significant wave height and the peak wave period were taken as $H_S = 4$ m and $T_p = 9$ s.

Because the simulations were done in the time domain, time series of the wind and the waves were needed. The wind speed time series was calculated by the software TurbSim. It calculates the wind speed at discrete points in a grid that covers the rotor plane area, for all time steps [36]. The time series for the waves was calculated by an internal function in Fedem Windpower. The same time series for the wind and the waves were used for all simulations.

3.2.4 Modelling of the wind turbine structure

Finite element beam elements were used to model the lattice tower. The discretization level is discussed in Section 3.3.

The rotor blades were represented by finite element beam elements, 40 elements per blade. Fedem Windpower uses the software AeroDyn to calculate forces on the blades. AeroDyn uses the wind speed time series calculated by TurbSim to calculate the loads on the rotor blades [37].

The foundation consists of four piles and each pile was modelled with ten beam elements. The soil was described by the so-called p–y-method, by represented the soil stiffness as nonlinear springs at the nodes. The soil profile was selected to match soil typically found in the North Sea [8].

The control system was implemented in the model. It was based on th NREL 5 MW reference turbine control system [38], but modified to suit a 10 MW turbine.

3.3 Element convergence study

The accuracy of the results from the simulation depends on the discretization level of the model. More finite elements will give more accurate descriptions of the mass and stiffness distributions. The natural frequencies have to be represented correctly for the dynamic analysis to give reliable results. In addition, the moments at the nodes need to be represented correctly because the joint fatigue lifetime is calculated from the joint stress time series.

The convergence of the natural frequencies and the moments was investigated for the simple beam from Section 3.1, as well as for the lattice tower.

3.3.1 Simple beam

Convergence of first natural frequency

The first natural frequency of the simple beam described in Section 3.1.1 was calculated when it was discretized into an increasing number of elements. The simulations were done with a marine growth thickness of 0.25 m, more than is considered realistic. Figure 3.3 shows the first natural frequency as a function of element discretization, normalized with respect to the exact value as calculated by Equation (3.3). From the figure, it is concluded that a discretization into four elements will give a good representation of the first natural frequency.

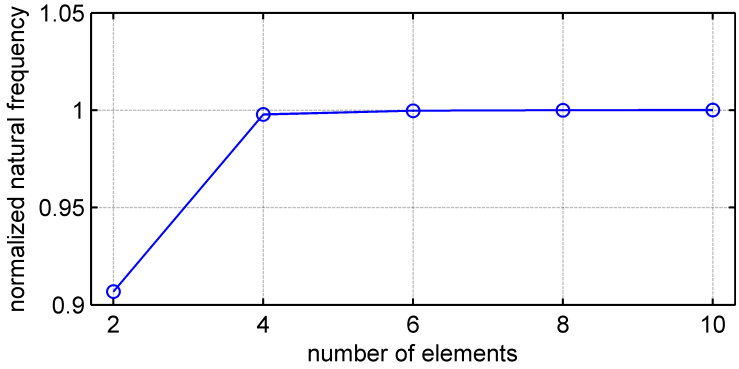

Figure 3.3: Convergence of first natural frequency for the simple beam.

Moment convergence

To study the convergence of the moment distribution, a load case of an evenly distributed load was used. The distributed load was lumped as point loads to the nodes manually. The ratio between the end moment and the moment at midspan was used as a indicator of convergence. In Figure 3.4, this ratio is plotted for an increasing discretization level. For comparison, the theoretical value is also shown. The figure shows that even for a discretization into ten elements, there is a discrepancy between the theoretical value and the result from the simulation. For a division of the beam into 10 elements, this error is 2.9 %. The acceptable discretization level depends upon the required accuracy.

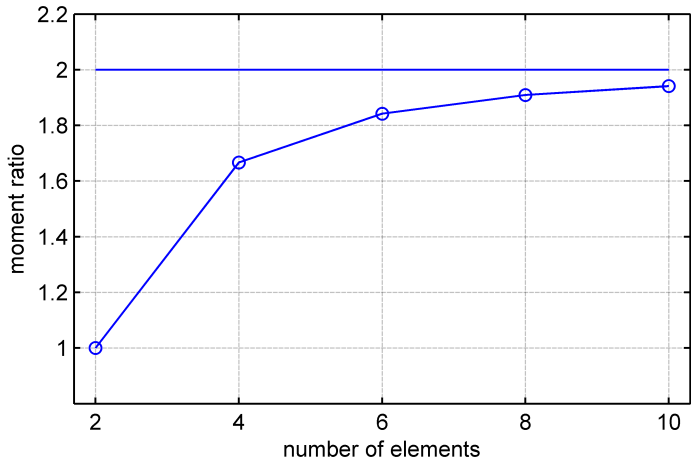

Figure 3.4: Convergence of moment ratio for the simple beam.

3.3.2 Lattice tower

In addition to the convergence study of the simple beam, a similar study was conducted on the lattice tower. For the lattice structure, the exact values of the natural frequencies and moment distribution are unavailable. The simulations were conducted with an increasing number of elements per member and 10 elements per member is used as a reference value.

Convergence of natural frequencies

Figure 3.5 shows the convergence of the first 20 natural frequencies. In general, the results are accurate even with few elements per member. With only element, the error in first natural frequency is only 0.03 %, and maximum error is 3.6 % for the fifth natural frequency. With two elements, the maximum error is less than 1.0 % for all of the considered natural frequencies. Two elements per member is considered sufficient to fulfill this discretization criterion.

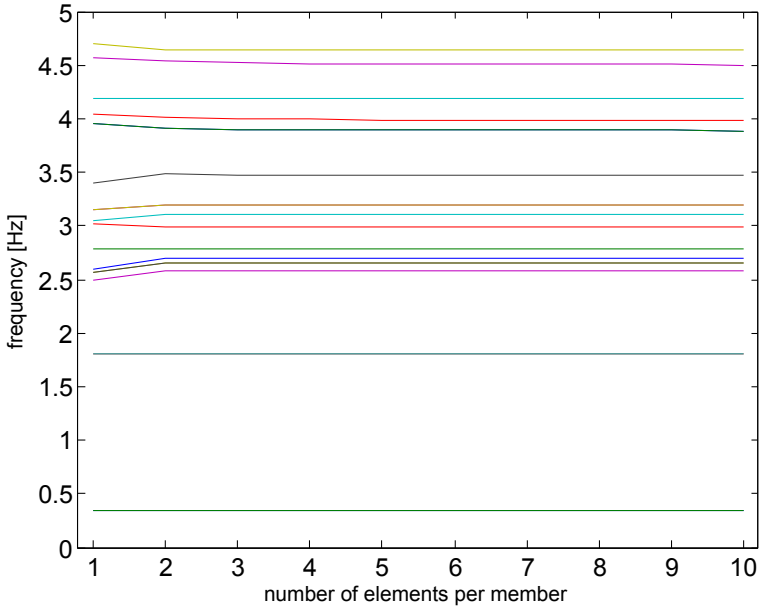

Figure 3.5: Convergence of natural frequencies for lattice tower.

Moment convergence

A load case with a steady current and no wind was used to investigate the convergence of the moment distribution. This results in a evenly distributed load on all members below the water line. The simulations were run for 1, 2, 4, 6, 8 and 10 elements per member. The axial force, in-plane and out-of-plane moments were normalized with respect to the results from the 10-element simulation.

As an example, the three plots for the braces in the K-joints are given in Figure 3.6. For the K-braces, mainly the moments are interesting. They are reasonably well represented with 4 – 6 elements. The normalized axial force converges slowly, but that is because the absolute value is low in the bracing. The corresponding plots for the leg and X-joint are given in Appendix B. It should be mentioned that the leg normal force is very well represented by two

elements. To represent brace bending, more elements are needed, but the results are considered acceptable with a discretization into six elements.

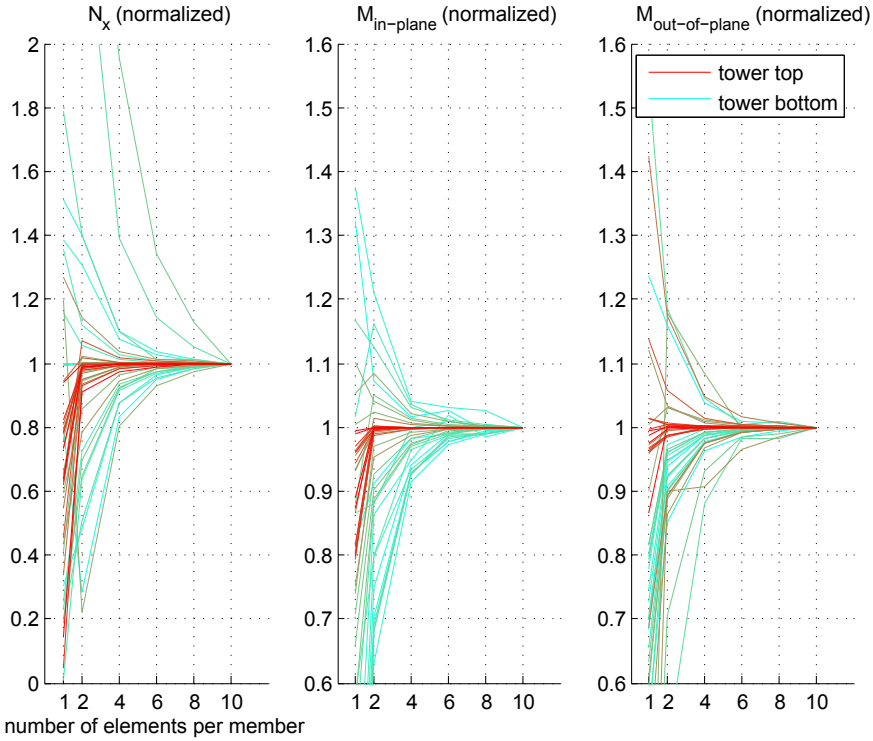

Figure 3.6: Convergence of axial force and moments for brace in K-joint.

3.3.3 Chosen discretization level

Since the convergence of the natural frequencies requires two elements per member and the moment criterion is fulfilled with six elements, the moment criterion will be governing. However, the moment distributions is only interesting for the members below the mean water level, so it is unnecessary to use six elements on members above the water level. A setup with six elements per member for the three lowermost sections and two elements per member for the rest of the

sections was suggested. The setup will minimize the computational cost while retaining the required accuracy.

To verify the computational savings for this 2/6-element setup, three cases were compared. The case with only two elements for all members constitutes the lower bound for computational cost, whereas the case with 6 elements for all members is the upper bound. The computational times for one simulation as described in Section 3.2 were found and the normalized computational times are shown in Table 3.6. The savings for the 2/6-element setup compared to the 6-element setup are considered so valuable that all further simulations were run with six elements for the three lowermost sections and two elements for the rest of the structure.

Table 3.6: Computational time for various discretization levels.

Number of elements per member	2	2/6	6
Computational time, normalized w.r.t. 2 elements	1	1.42	2.40
Computational time, normalized w.r.t. 6 elements	0.42	0.59	1

3.4 The FL and SEC load cases

3.4.1 Presentation of the load cases

The load cases FL0.050 to FL0.20 represent marine growth uniformly distributed over the *full length* below the mean water level, with thickness as specified in the load case name, as seen in Table 3.7.

Table 3.7: Description of the FL load cases.

Section number	Depth range [m]	Applied MGT [m] FL0.05	FL0.10	FL0.15	FL0.20
3	–2 - 15	0.05	0.10	0.15	0.20
2	15 - 36	0.05	0.10	0.15	0.20
1	36 - 60	0.05	0.10	0.15	0.20

For the load cases where marine growth is applied *section*-wise, the marine

growth thickness is specified to 0.10 m. The sections where marine growth is applied are mentioned in the load case name, as seen in Table 3.8. Recall that section 1 is the lowermost section.

Table 3.8: Description of the SEC load cases.

Section number	Depth range [m]	Applied MGT [m] SEC3	SEC2+3	FL0.10	SEC1+2	SEC1
3	–2 - 15	0.10	0.10	0.10	0	0
2	15 - 36	0	0.10	0.10	0.10	0
1	36 - 60	0	0	0.10	0.10	0.10

3.4.2 Interpretation of the load cases

Based on the scenarios proposed by Oldfield (ed.) [2], see Section 2.5.2, three characteristic situations are proposed.

MD: Mussel Dominated
Represents a location in the mussel dominated zone close to shore. Dense mussel fouling in the upper 30 m of the structure; and also below 30 m, fouling is relatively dense.

OUB: Offshore Upper Bound
Represents the upper bound for a structure placed further offshore, in the central region of the North Sea. A relatively thick layer of mussel fouling is assumed, as well as dense growth below 30 m.

OLB: Offshore Lower Bound
Represents the lower bound for a structure placed further offshore, in the central region of the North Sea. Both mussel fouling and fouling below 30 m is limited.

Table 3.9: Marine growth levels after 7 to 8 years in water.

Depth range [m]	Applied MGT [m] MD	OUB	OLB
0 – 30	0.20	0.15	0.08
30 – 60	0.60	0.11	0.06

With these predictions in mind, it is possible to interpret the load cases presented in the preceding section.

The FL load cases represent reference cases. They enable comparing the effect marine growth has on different structures with various design, founded at different depths, with different number of sections, etc. However, it is seen from Table 3.9 that FL0.20 is an unrealistic load case, as dense mussel fouling is not found below 30 m depth.

The SEC load cases are more specific to this lattice tower. Since SEC2+3 has marine growth down to 36 m, this resembles a realistic situation with mussel dominated fouling. SEC1 and SEC1+2 may represent a situation where cleaning of the braces of the uppermost section(s) has been performed.

Chapter 4

Results

4.1 Terminology and reference points

Figure 4.1 shows the geometry of the lattice tower. The front and side views are identical and the brace angle is constant, implying that the section height varies over the tower height. The figure defines some important terms. *K-brace* is used for the brace in a K-joint, and *K-leg* is used for the leg. *X-brace* denotes the joint where two diagonal braces meet.

Figure 4.1 also marks the reference points that will be referred to throughout the rest of the report, when the results are presented. The reference points are found in the first and third section. All points are found on the upwind side of the tower. The points are named RPX1, RPK1, RPX3 and RPK3 where RP means reference point, X or K denotes X- or K-joint and the number represents the section number.

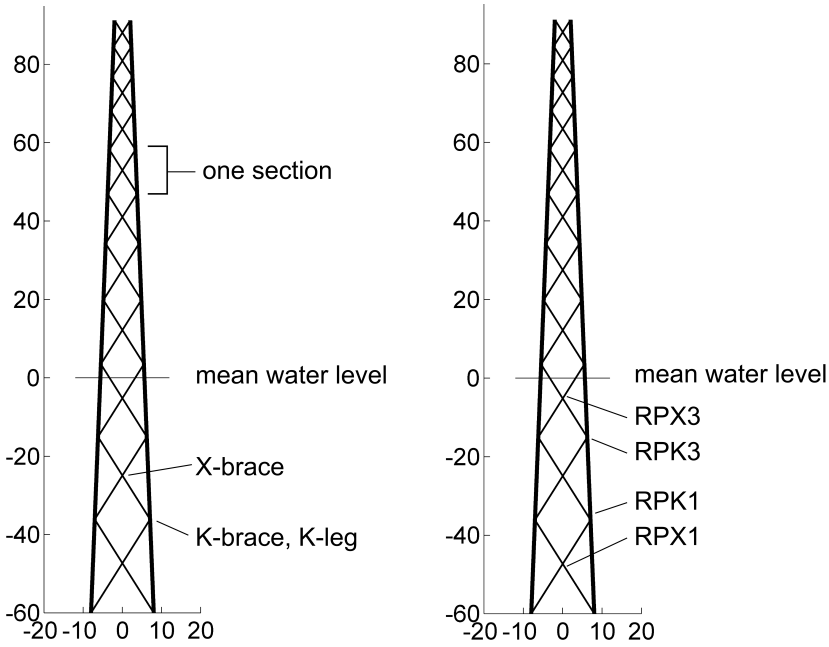

Figure 4.1: Terminology and position of the reference points.

4.2 Mode shapes and natural frequencies

In this section, the mode shapes and natural frequencies of the lattice tower will be presented. Representing the reference case, marine growth is neglected.

The 12 first mode shapes and natural frequencies are presented in Table 4.1 and the modes shapes are depicted and in Figure 4.2. The mode shapes are ordered by increasing natural frequency and each mode shape is labelled with a letter. The meaning of "flower-symmetric", "dog bone-symmetric" and "asymmetric" brace modes can be understood from the top views in the figure.

Using the illustrations in Figure 4.2, it is possible to identify global and local mode shapes:

Global mode shapes: A, B, F, G

Local mode shapes: C, D, E, H, I, J, K, L

Some of the mode shapes defined as local modes also include some global deformation. This includes modes D, I, J, K.

Table 4.1: Natural frequencies of the lattice tower.

	Mode shape description	Natural frequency [Hz]
A	Global cantilever	0.344
B	Global top fixed	1.80
C	1st bay dog bone-symmetric brace	2.59
D	1st bay asymmetric brace	2.65
E	1st bay flower-symmetric brace	2.69
F	Global torsion	2.78
G	Global diagonal “flattening”	2.99
H	2nd bay dog bone-symmetric brace	3.11
I	2nd bay asymmetric brace	3.19
J	2nd bay flower-symmetric brace	3.48
K	2nd and 3rd bay opposite asymmetric brace	3.89
L	3rd bay dog bone-symmetric brace	3.98

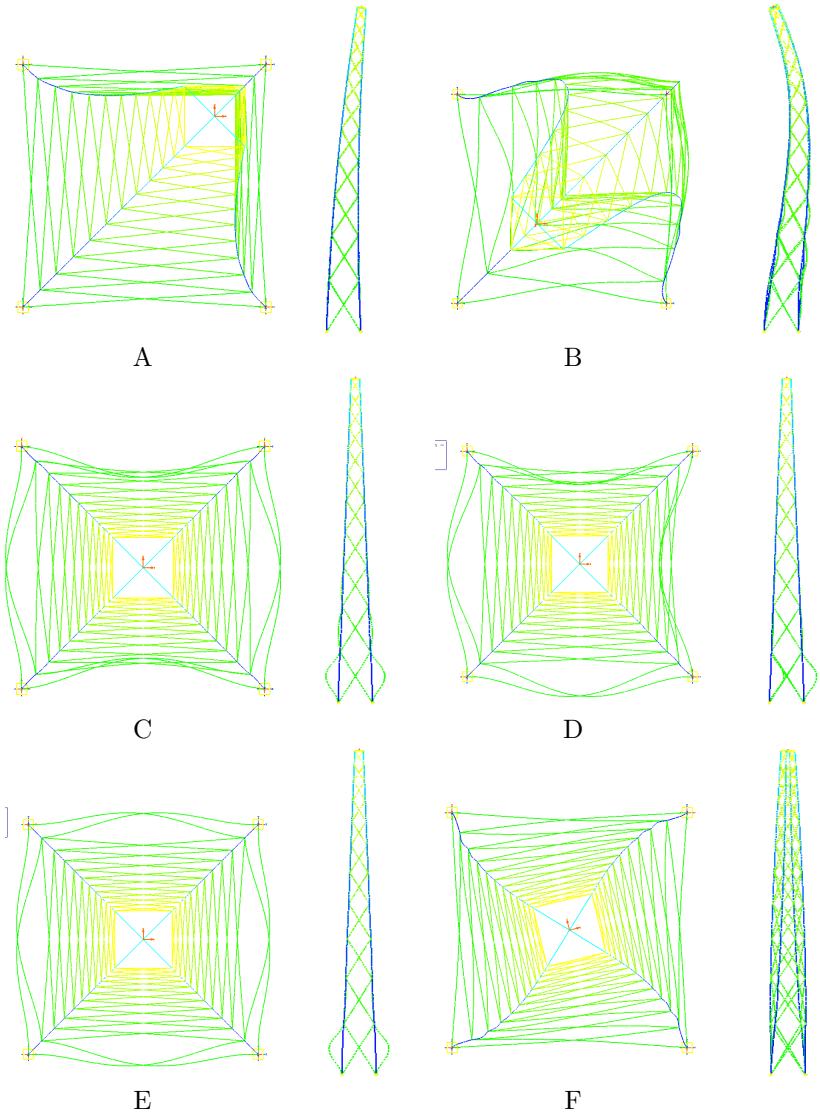

Figure 4.2: The 12 first mode shapes of the lattice tower (continues).

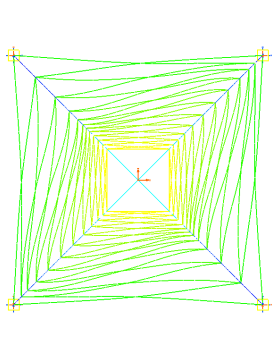

G

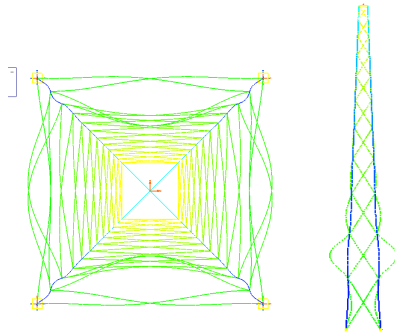

H

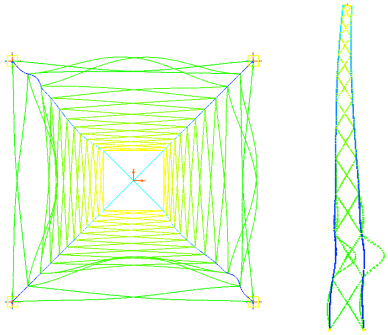

I

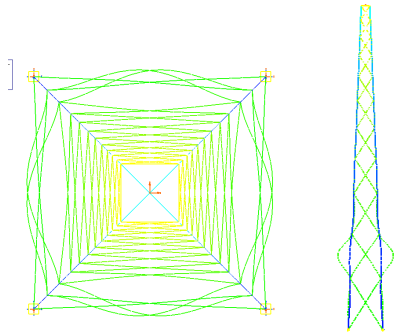

J

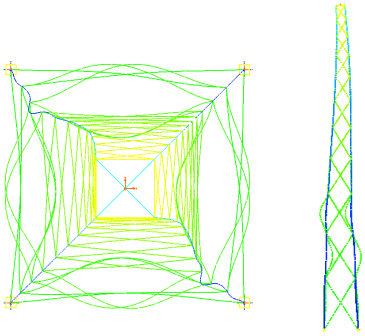

K

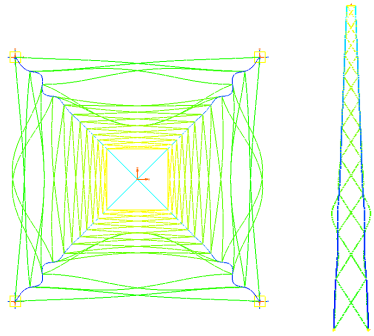

L

4.3 Natural frequencies: Effect of marine growth

4.3.1 Uniformly distributed marine growth

Marine growth was applied uniformly on the three lowermost sections of the lattice tower. The effect on the the natural frequencies is presented in Figure 4.3 and Table 4.2.

In the following discussion, the modes are grouped as follows for simplicity: Modes C, D and E are referred to as the 1st bay group; Modes H, I and J are referred to as the 2nd bay group; Modes K and L are left out. With this classification, the natural frequencies (calculated with no marine growth) differ less than 12 % within each group. Also, the change in natural frequency with marine growth differ less than 9 % for the maximun applied marine growth. This is considered sufficiently accurate for the discussion. Non-averaged results may be found in Appendix C.

Table 4.2: Change in natural frequencies for the FL load cases.

	Mode description	Relative change in frequency [%]			
		FL0.05	FL0.10	FL0.15	FL0.20
A	Global cantilever	0.0	-0.1	-0.2	-0.3
B	Global top fixed	-3.0	-6.8	-11.5	-18.2
1st	1st bay local modes	-12.7	-24.8	-34.0	-40.9
F	Global torsion	-4.4	-9.0	-13.8	-18.4
G	Global diagonal “flattening”	-7.7	-14.3	-20.4	-26.0
2nd	2nd bay local modes	-12.8	-24.1	-32.9	-39.8

From Figure 4.3 and Table 4.2, it is clear that the local modes are are more sensitive to changes in marine growth than the global modes. Marine growth has negligible effect on the first natural frequency. The natural frequency for modes B and F both experience less than 20 % decrease for 0.20 m growth. The effect on mode G is larger, but still significantly smaller than the effect on the local modes. The relative change in natural frequency is very similar for the 1st bay and the 2nd bay local mode groups. For a thickness of 0.10 m, the relative change is around 24 % and for 0.20 m it is around 40 %.

The change in the first natural frequency is less than predicted in Table 3.3.

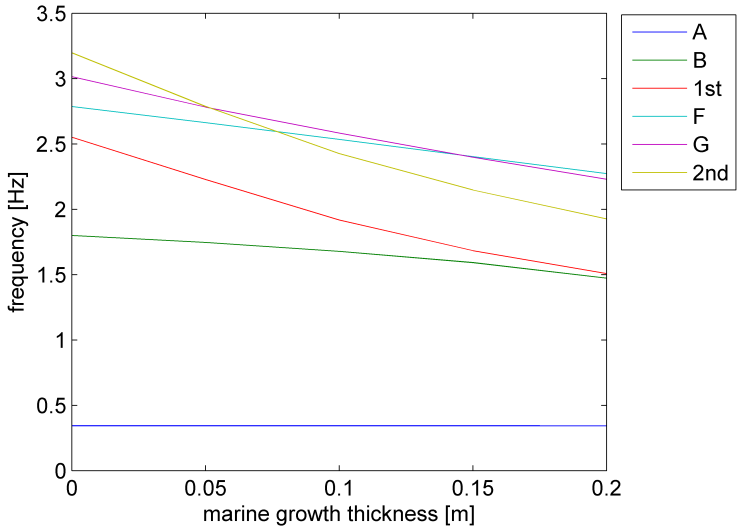

Figure 4.3: Natural frequencies of the lattice tower for the FL load case.

The changes in local mode natural frequencies are very close to the predictions made in Table 3.4.

Because the different relative change in natural frequency, the modes are permuted in their order when sorted by frequency. This has been possible to take into account by recognizing the mode shapes from the deformation plots. Although permuted in their order, the modes keep their shape when marine growth is applied. The exception is mode L, which changes from being a 2nd and 3rd bay local mode to a 3rd bay only local mode, already with 0.05 m growth.

4.3.2 Section wise distributed marine growth

0.10 m marine growth

Marine growth with thickness was applied to the bays as described in Table 3.8, such that SEC1 means applied on the 1st bay etc. The resulting relative change in natural frequency is presented in Table 4.3. Also in this section, mean values

have been calculated for the 1st bay and the 2nd bay groups; non-averaged results may be found in Appendix C.

Table 4.3: Change in natural frequencies for the SEC load cases.

Mode label	Mode description	Relative change in natural frequency [%]				
		SEC3	SEC2+3	FL0.10	SEC1+2	SEC1
A	Global cantilever	-0.1	-0.1	-0.1	0.0	0.0
B	Global top fixed	-4.2	-6.6	-6.9	-3.0	-0.5
1st	1st bay local modes	-0.2	-8.9	-27.5	-27.4	-27.3
F	Global torsion	-4.7	-8.3	-8.9	-4.7	-0.6
G	Global "flattening"	-8.2	-12.9	-13.5	-6.9	-0.7
2nd	2nd bay local modes	-9.3	-18.3	-25.6	-25.3	-0.5

From Table 4.3, it is seen that for SEC3, mainly the 2nd bay local modes and the global diagonal "flattening" mode will be affected. The cases SEC2+3 and FL.10 yield similar results for the global modes, but FL0.10 has larger effect on the local modes. The case SEC1 will affect the 1st bay local modes only. However, the effect on this group will be the same as for the uniformly distributed case. The same reasoning holds for SEC1+2.

The most important result is that for all natural frequencies, the change is largest when marine growth is applied uniformly over the three lower bays. This means that an eigenfrequency analysis with uniformly distributed growth will be conservative.

0.20 m marine growth

Eigenfrequency analyses have been performed with distribution corresponding to that showed in Table 3.8, but with 0.2 m marine growth.

In this case, inspection of the mode shapes revealed that they change to a much larger extent in this case. New shapes are introduced whereas others disappear. This means that it has been meaningless to quantify the relative change in natural frequency and that grouping of the mode shapes has been impossible. Therefore, only a quantitative description will be given.

A general observation is that when marine growth is applied to a specific bay,

the local modes corresponding to this bay are favoured by having their natural frequencies reduced.

When marine growth is applied to bays 1+2 or 1, all 1st bay local modes will have a natural frequency less of that corresponding to B: global top fixed. Also, there will be no 3rd bay local modes among the 20 first modes. Instead, new modes involving both bays 1 and 2 are introduced. When marine growth is applied to bays 2+3, the 2nd bay local modes will have frequencies smaller than those in the 1st bay group.

4.4 Comparison of natural and loading frequencies

4.4.1 Wind loads

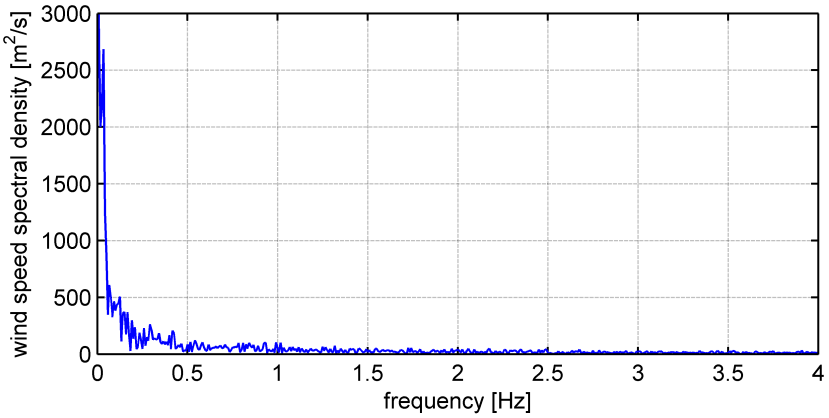

Figure 4.4: Spectrum for wind speed used in the simulations.

Figure 4.4 shows the frequency spectrum for the wind speed time series that was used in the simulations. Most of the wind consists of frequencies less than 1.0 Hz. Only the first natural frequency of the lattice tower $f = 0.344$ Hz falls within this frequency range.

4.4.2 Wave loads

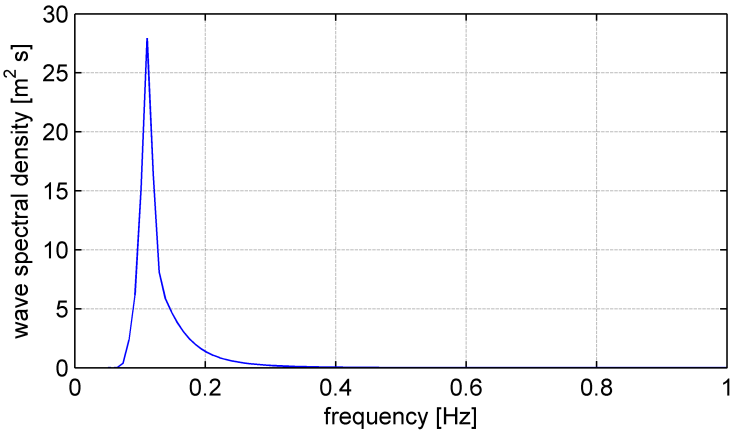

Figure 4.5: Wave spectrum used in the simulations.

Figure 4.5 shows the JONSWAP wave spectrum that was used in the simulations. The waves have frequencies$f \leq 0.3$ Hz, lower than the first natural frequency $f = 0.344$ Hz.

4.4.3 Harmonic loads from the wind turbine

In Figure 4.6, the natural frequencies of the structure are compared to the P-values of the turbine. The plotted P-values are the actual range of each P-value found are from the analysis results. They are within the theoretical P-values for the turbine, as explained in Section 2.1.2.

It is seen that the values for 1P, 3P and 6P are well separated from the natural frequency values. The first natural frequency lies between the 1P and 3P values, indicating that the lattice tower has a so-called “soft-stiff” design.

Where one or more natural frequency is within a nP-range, dynamic amplification may occur. For the 9P and 12P-ranges this is the case for almost all values of marine growth thickness. The exceptions are FL0.15 for 9P and 0.2 for 12P.

Where two or more natural frequency values are close or coincide, interaction between the two modes may cause dynamic amplification.

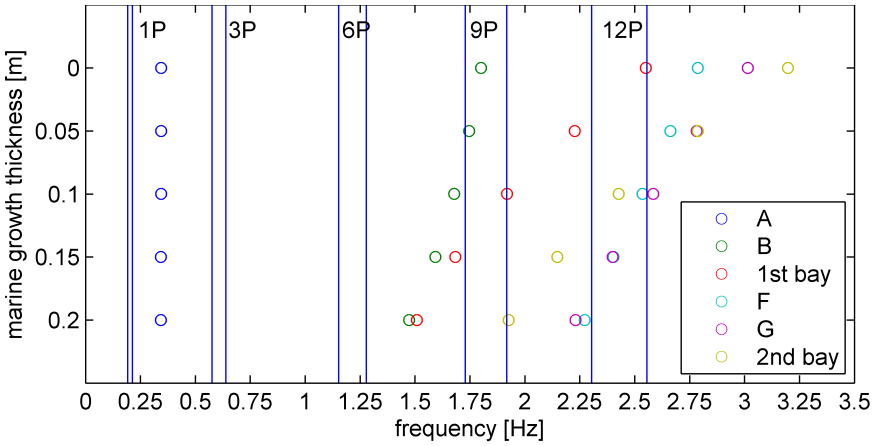

Figure 4.6: Comparison of nP-values with the natural frequencies.

4.5 Variance spectrum of out-of-plane deformation

In Figure 4.7, the variance spectrum for the out-of-plane displacement of RPX1 is given. The variance spectrum was made by a fast Fourier transform of the time series of the displacement, when the misleading results from the start-up were discarded, as described in Section 3.2.2. The red vertical lines represent the ranges of the nP-values as explained in Section 4.4.

Three spectra are given, calculated with for simulations including both wind and waves, no wind and no waves respectively. In the spectrum calculated with only waves, two peaks are found at $f = 0.09$ Hz and f 0.32 Hz, corresponding to the JONSWAP peak period $T_p = 9$ s as well as the first natural frequency of the tower $f = 0.344$ Hz. The spectrum calculated with only wind closely resembles that calculated with both wind and waves.

In Section 3.1.4, it was shown that marine growth will cause a large increase in wave loading for member dimensions relevant for the lattice tower. However, from Figure 4.7, it is clear that the contribution from the waves to the spectrum is small compared to that of the wind loads. Therefore, it may be expected that the increased wave loads will have limited influence on the fatigue life.

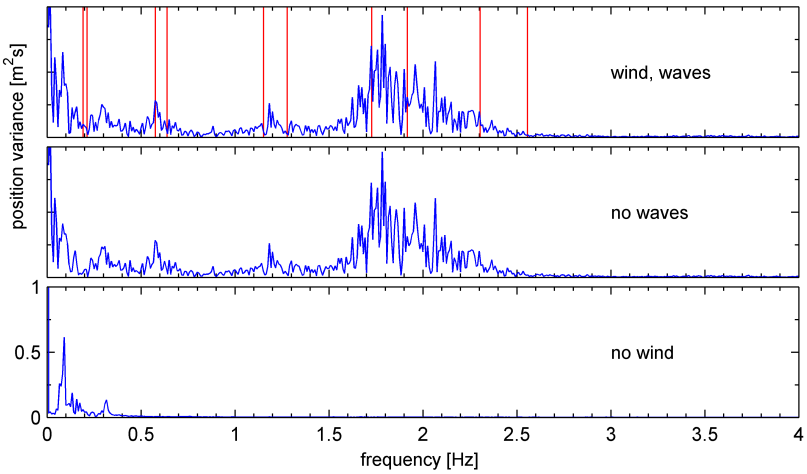

Figure 4.7: Variance spectrum for out-of-plane displacement of RPX1.

A plot that shows the low-frequency response more clearly, as well as the corresponding plot for RPX3 is given in Appendix D.

4.6 Stress spectra for the FL load cases

4.6.1 Normal stresses

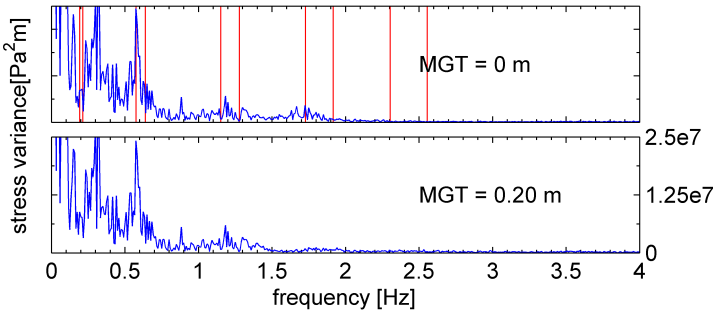

Figure 4.8: Variance spectrum for leg normal stress in the leg at RPK1.

The variance spectrum from the fast Fourier transform of the normal stress in the leg at RPK1 is given in Figure 4.8. The red vertical lines represent the ranges of the nP-values as explained in Section 4.4. It is seen that the response is negligible for frequencies $f \geq 2.0$ Hz. A small peak can be recognized at 6P and the peak at 3P is larger. Most of the response has frequency $f \leq 0.6$ Hz. Around $f = 0.344$ Hz, the first global mode, the response is also high. Deformation corresponding to this fore-aft mode will give global bending and normal stresses in the legs.

The spectrum for RPK3 is as expected almost identical, except that the response is even smaller for $f > 0.6$ Hz. The plot is given in Appendix E.

For both reference points, the spectra found for no marine growth and FL0.20 are almost identical. It is concluded that the effect of marine growth on the normal stresses in the legs is negligible.

4.6.2 Out-of-plane stresses

The variance spectra for the out-of-plane stresses for RPK1, RPX1, RPK3 and RPX3 are given in the Figures 4.9 through 4.12.

All plots show a peak around $f \approx 0.15$. This peak is expected to be caused by the waves, as the wave peak period is $T_p = 9$ s. The peak increases with increasing marine growth thickness for all plots. For RPK3 and RPX3, the points in the section immediately below the mean water level, this peak covers a broader frequency range.

Also, peaks are found around frequencies corresponding to 3P, 6P and 9P for all reference points. The peak at 3P is in general small, but recognizable. The amplitude is constant or increases modestly with increasing marine growth. The peak at 6P is small with no marine growth, but increases significantly for all the considered reference points. This could not be predicted from Figure 4.6. The peak around 9P is high, even with no marine growth. It was seen from Figure 4.6 that the 9P-value may have some interference with one or more natural frequency value for more or less all marine growth thicknesses. This might be the cause for the high Fourier amplitudes in this frequency range. Then, dynamic amplification should also be expected around the 12P. However, the 12P-peak is difficult, if not impossible, to distinguish.

In addition to the effect on these peaks, the plots show that with increasing marine growth, the Fourier amplitudes increase to varying extent in the frequency range from $f = 1.2$ Hz to $f = 3$ Hz .

The variance spectra for the out-of-plane stresses for the X-braces are given in Figures 4.9 and 4.10. The spectrum for point RPX1 is a more narrow-banded spectrum than the one for RPX3. There is a shift from higher to lower frequency with increasing marine growth. Comparing with Figure 4.6, it looks like the variance spectrum has high amplitudes where the 1st bay local modes have interference with the 9P range, for marine growth thickness 0.10 m and 0.15 m. For FL0.20, the B: global top fixed and the 1st bay local mode natural frequencies coincide and are then at their closest to the 6P-range. Although the frequencies are still well separated, it looks like this causes dynamic amplification. For reference point PRX3, the variance increases at a broad frequency range with increasing marine growth thickness. However, the variance is unchanged around 9P and increases more around 6P.

The variance spectra for the out-of-plane stresses for the K-braces are given in the figures 4.11 and 4.12. Both spectra have a broad-banded appearance for no marine growth. For RPK1, the amplitudes increase especially much in the 6P and the 9P-ranges. In the range $f = 2.2$–2.4 Hz, the amplitudes are especially high for FL0.10 and FL0.15. This may be an effect of that several of the natural frequencies are within the 12P-range for these marine growth thickness values,

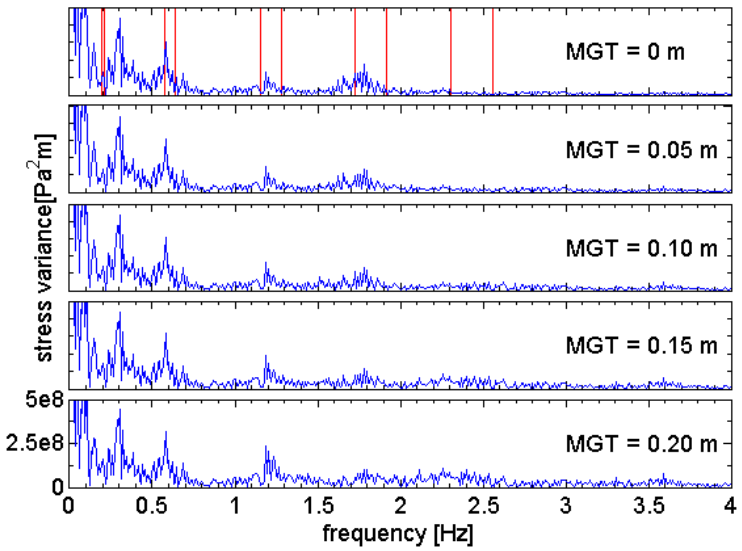

Figure 4.9: Variance spectrum for out-of-plane stress in RPX1.

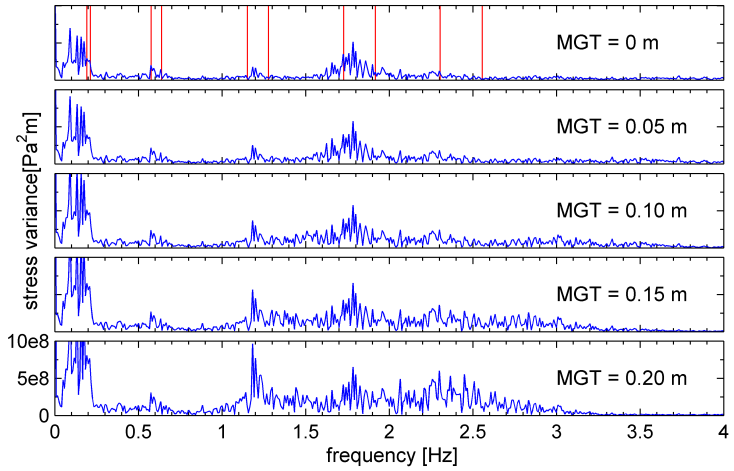

Figure 4.10: Variance spectrum for out-of-plane stress in RPX3.

see Figure 4.6. The spectrum gets more narrow-banded as the marine growth thickness increases. The Fourier amplitudes in the stress spectrum for RPK3 increases more evenly and the spectrum preserves the broad-banded appearance.

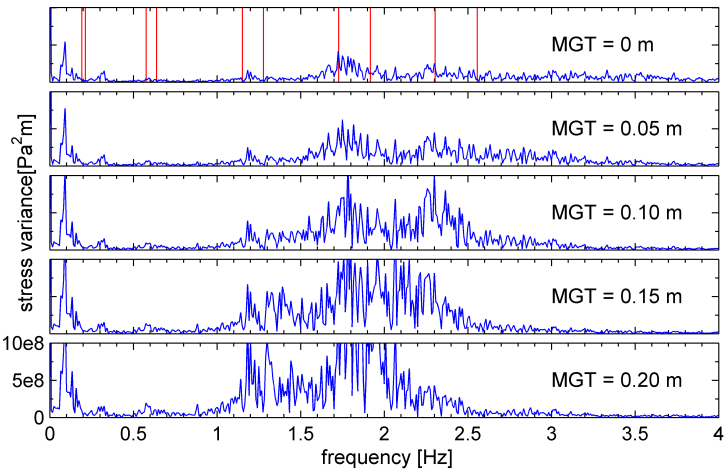

Figure 4.11: Variance spectrum for out-of-plane stress in RPK1.

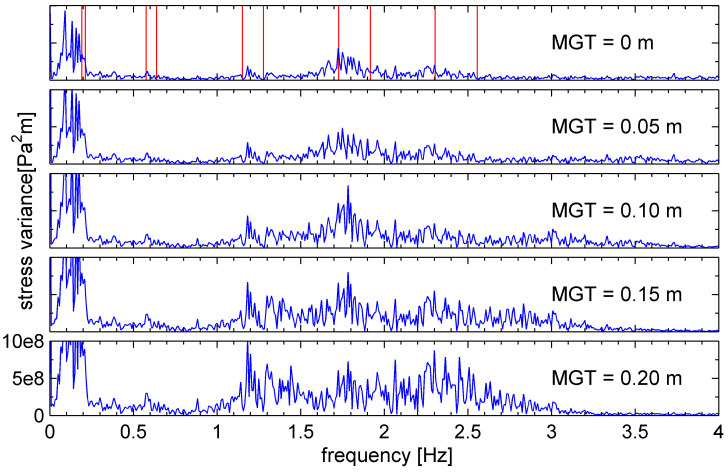

Figure 4.12: Variance spectrum for out-of-plane stress in RPK3.

4.6.3 In-plane stresses

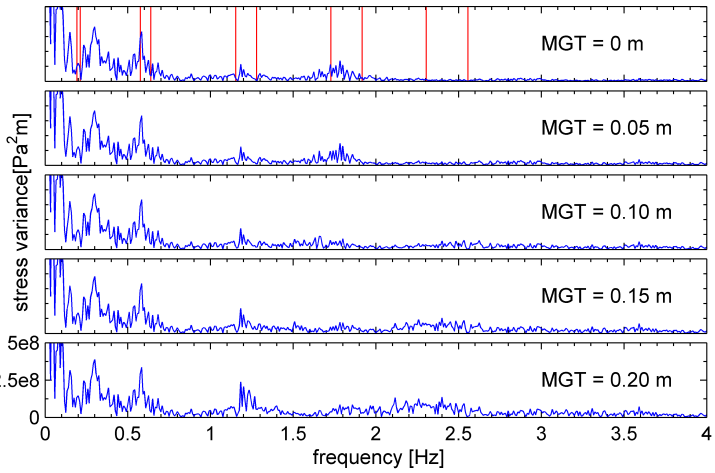

Figure 4.13: Variance spectrum for brace in-plane stress in RPK1.

The variance spectrum for in-plane stresses for RPK1 is given in Figure 4.13. Note that the y-axis is modified compared with the corresponding plots for the out-of-plane stresses. It is seen that the Fourier amplitudes are unchanged for frequencies $f \leq 1$ Hz. With increasing marine growth, the amplitudes increase around the 6P-peak, whereas they decrease in the 9P and 12P-ranges.

The corresponding plots for the other reference points are given in Appendix E. In general, they show similar characteristics as the one for reference point 106. The peaks at 3P and 6P are small, but recognizable. The 9P and 12P-peaks are more difficult to distinguish. In general, the in-plane stresses show little sensitivity to increasing marine growth, although not totally unaffected.

4.6.4 Decomposition of the frequency plots

To further investigate the behaviour of the structure, the two effects marine growth has on the structure were separated. In one group of simulations, only the increased member diameter was taken into account, by setting the mass

density of marine growth to zero. Then, marine growth will only increase the wave loads. In the following discussion, the curves for this group are plotted in *green*. The other group of simulations includes only the additional mass of the marine growth, not increasing the member diameter by the common two times marine growth thickness. The curves from this group of simulations are plotted in *red*. The simulations were conducted for marine growth thickness of 0.10 m and 0.20 m.

As the marine growth has little effect on the in-plane stresses, this discussion will consider out-of-plane stresses only.

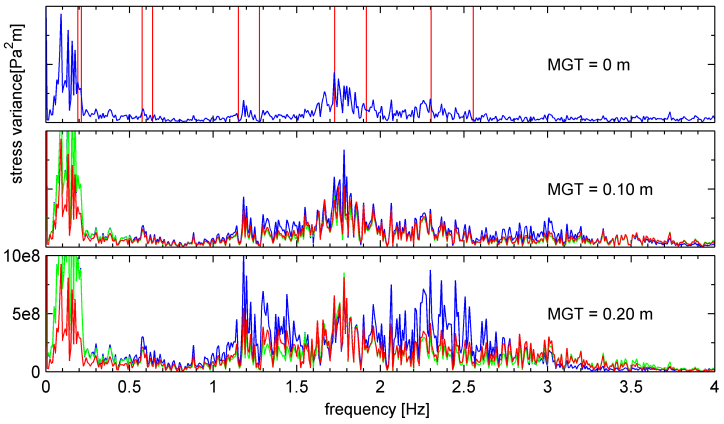

Figure 4.14: Variance spectrum for out-of-plane stress in RPK3. Comparison of three setups.

In Figure 4.14, the curves from the three groups of simulations are plotted for RPK3. The peak around $f \approx 0.15$ Hz is identical for the total analysis and the analyses that only take the increased diameter into account. This confirms that the peak is caused by wave loads. For the frequencies $f > 0.2$ Hz, the amplitudes of the total model is higher than each of the two other models, except for high frequencies, $f < 2.75$ Hz.

In Figure 4.15, the variance spectra for the simulations only taking the increased diameter into account are plotted for RPK3. The response for the total model for *no marine growth* is plotted in blue as a reference . The corresponding plots for the simulations taking only the increased mass into account are shown in

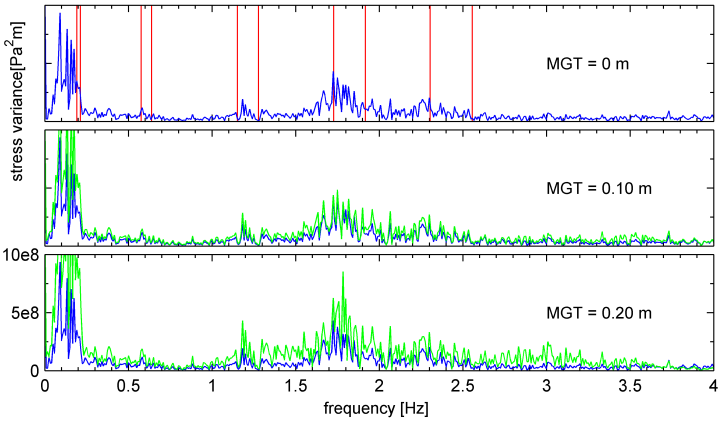

Figure 4.15: Variance spectrum for out-of-plane stress in RPK3. Effect of increased diameter.

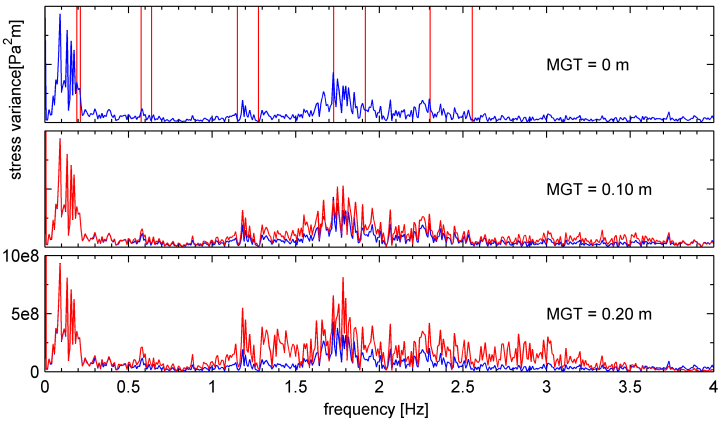

Figure 4.16: Variance spectrum for out-of-plane stress in RPK3. Effect of additional mass.

Figure 4.16.

For frequencies $f > 0.2$, the curves for the two "decomposed" simulations are in general quite similar. They are more similar to each other than they resemble the curve for the total response. The variance increases at all frequencies between $f = 0.2$ Hz and $f \approx 3.75$ Hz, though more around 6P and 9P-frequencies. For the analyses that take only additional mass into account, the peak around $f \approx 0.15$ Hz is unchanged with increasing marine growth thickness. At this low frequency, the dynamics of the structure are less important.

The corresponding three plots are given for all reference points in Appendix E. In general, the two analyses including only one effect each are more similar to each other, than to the total model. The peak around $f \approx 0.15$ Hz is unchanged with increasing marine growth thickness for the analyses that take only the additional mass into account. The increase in the total response is equal to the response in the model taking only increased diameter into account for the low frequency range. Neither of the two "decomposed" simulations give sufficiently accurate predictions to the total response, except from in the lowest frequency range. Both effects must be included if the dynamic behaviour shall be described correctly.

4.7 Fatigue lifetime for the FL load cases

4.7.1 Lifetime of the three lowermost sections

In Figure 4.17, the joint fatigue lifetime of the X-braces, K-braces and K-legs of the three lowermost sections is plotted. The lifetime is taken as the lowest lifetime of all the X-braces, K-braces and K-legs in the respective section.

The lifetime of the X-braces and K-braces decrease with increasing marine growth thickness. For all sections, the lifetime of the K-braces is higher than that of the X-braces. However, the K-brace lifetime decreases more than the X-brace lifetime such that the lifetime values approach each other with increasing marine growth thickness. The K-leg lifetime shows more irregular behaviour. With an intermediate marine growth thickness, the K-leg lifetime increases, but for FL0.20, the lifetime is significantly reduced. Thus, applying a marine growth thickness of 0.10 m may overestimate the K-leg lifetime.

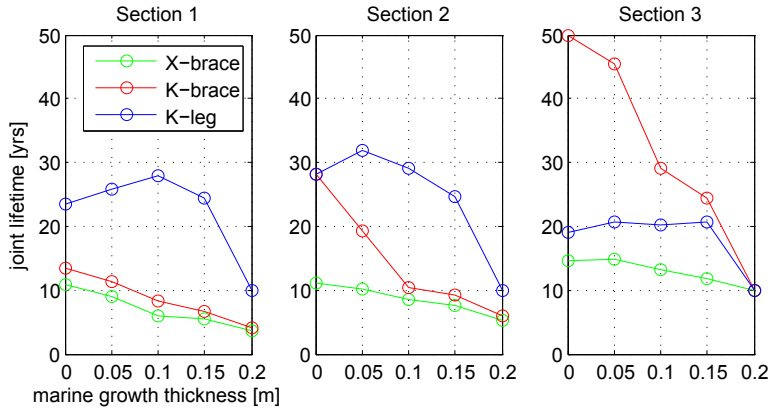

Figure 4.17: Joint fatigue lifetime for the FL load cases.

For the three lowermost sections, the design lifetime will be governed by the X-braces for all the considered values of marine growth thickness. The X-braces in section 1 experience a reduction in lifetime of 44.1 % and 66.8 % for FL0.10 and FL0.20 respectively. This is a significant reduction in lifetime. The importance of the K-leg and K-brace fatigue lifetime increase as their lifetime values decrease. It would be interesting to run optimization analyses with marine growth implemented in the model.

4.7.2 Lifetime of the "decomposed" models

In Figure 4.18, the fatigue lifetime of the X-braces, K-braces and K-legs for the three lowermost sections. In addition, the fatigue lifetime for the "decomposed" models are plotted, that is, when only increased diameter and additional mass are implemented in the model respectively.

From the Figure, we observe that the analyses with both contributions gives significantly lower lifetime than each of those which only includes one effect. In Section 4.6.4, it was shown that the Fourier amplitudes of the stress spectrum were in general too low for each of the "decomposed" models. Therefore, it should be expected that the lifetime from the model with both effects is lower than each of the other two simulations. This holds, except for K-leg in section 1.

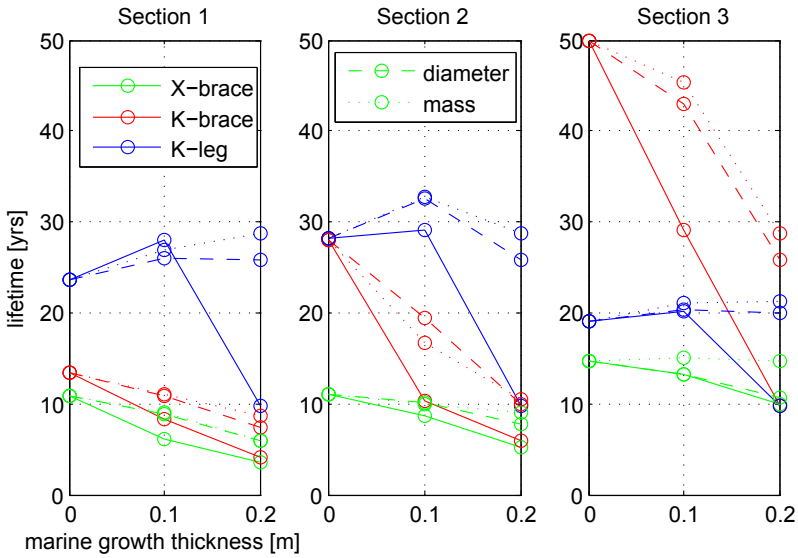

Figure 4.18: Joint fatigue lifetime. Comparison of three setups.

Especially for marine growth level of 0.20 m, there is considerable discrepancy between the lifetime calculated for the two "decomposed" models on the one hand and the total model on the other hand.

4.8 Fatigue lifetime for SEC load cases

4.8.1 Marine growth on the uppermost sections

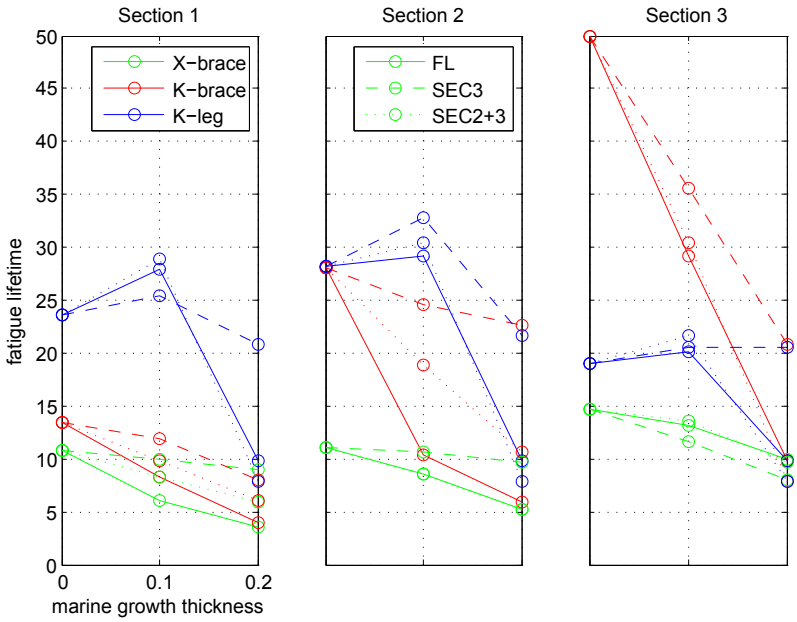

Figure 4.19: Joint fatigue lifetime for the SEC load cases.

In Figure 4.19, the fatigue lifetime of the X-braces, K-braces and K-legs are plotted for section wise distributed marine growth (SEC3, SEC2+3). The result for uniformly distributed marine growth (FL) is plotted as a reference.

It is expected that FL and SEC2+3 will yield similar results. In general, this is confirmed from the plots. There are two notable exceptions. For the K-brace

in section 2, the lifetime calculated for FL is about 50 % of that calculated for SEC2+3. Also, both the X-brace and K-brace lifetime in section 1 is considerable lower for FL than for SEC2+3.

In general, the lifetime calculated for SEC3 is significantly higher than the other two, but there are exceptions, as the X-brace lifetime in section 3.

It is interesting that FL does not always give conservative values. In Section 4.3.2, it was concluded that for marine growth levels of 0.10 m, the FL loadcase would always give the largest or equal change in eigenfrequency, when compared to the SEC loadcases. However, from Figure 4.19, it is evident that SEC3 or SEC2+3 may give lower lifetime values than the FL load case. For the K-leg and marine growth thickness 0.20, SEC2+3 gives 19.3 % lower lifetime for all sections. Also, for the section 3 X-brace, the lifetime for SEC2+3 is 18.6 % below the lifetime calculated for FL.

In this context, it can be useful to recall that, from Equation (2.25), a doubling of the stress amplitudes will increase the fatigue damage by a factor $2^5 = 32$ or $2^3 = 8$ depending on stress level. Therefore, small changes in stresses cause large scatter in fatigue lifetime.

As noted in Section 3.4.2, 0.20 m marine growth is unrealistic for the whole structure; SEC2+3 is more realistic for this marine growth level. As we have seen, these two cases in general yield similar results. However, following this argumentations, it is unfortunate that the lifetimes calculated for FL and 0.20 m are not conservative with respect to SEC2+3 and the same marine growth level.

4.8.2 Marine growth on the lowermost part

In Figure 4.20, the joint fatigue lifetime of the X-braces, K-braces and K-legs are plotted for section wise distributed marine growth (SEC1, SEC1+2) together with uniformly distributed marine growth (FL) as a reference. As mentioned in Section 3.4.2, marine growth applied on the lowermost sections may represent the result of some cleaning programme, when the marine growth is removed down to some specified depth.

In Section 4.3.2, it was shown that when marine growth was applied only on section 1 (SEC1), only the 1st bay local-mode natural frequencies were affected. In addition, the wave motion and the resulting wave loads are small at this depth. For these reasons, it is expected that SEC1 lifetime is little sensitive

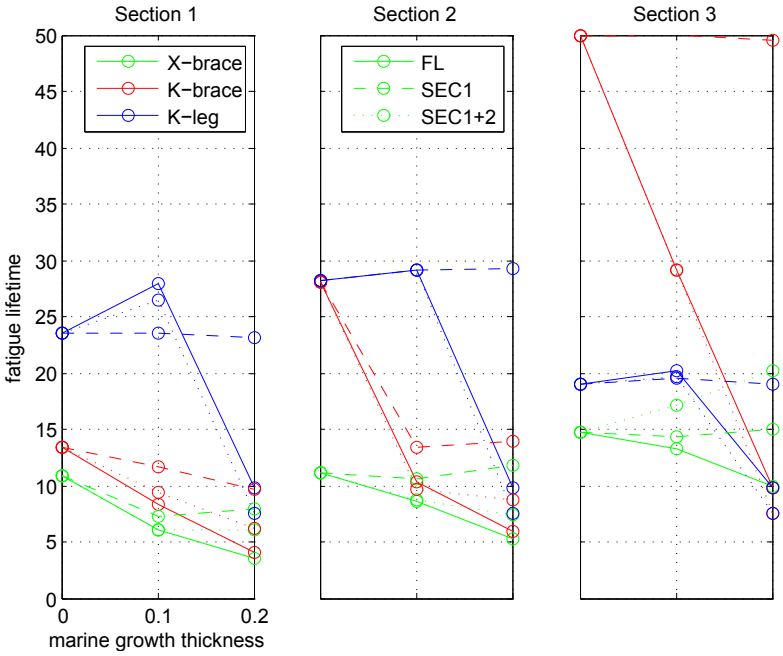

Figure 4.20: Joint fatigue lifetime for the SEC load cases.

to changes in marine growth. This is in general confirmed by the SEC1 curves in Figure 4.20. However, both the X-brace and K-brace lifetime of section 1 is significantly reduced. More surprisingly, the section 2 K-brace lifetime is also reduced.

The load case SEC1 0.10 m resembles cleaning of the two uppermost sections, a quite realistic situation. If this load case would give the same results as for no marine growth, marine growth considerations would be unnecessary, when following such a programme. However, at three points in Figure 4.20, this is not fulfilled; K-braces in section 2, X- and K-braces in section 3. Thus, if a cleaning regime is proposed, it is necessary to check the design with marine growth applied below the depth where cleaning is preformed.

In general, the FL and SEC1+2 cases yield similar results. The section 3 X-brace lifetime increases for SEC1+2.

It is again interesting to see if FL gives conservative results. The K-leg lifetime calculated for 0.20 m is in general a little lower for SEC1+2 than FL. This is also the case for section 3 K-brace lifetime for 0.20 m. However, as noted in Section 3.4.2, a marine growth level of 0.20 m is unrealistic for both SEC1 and SEC1+2 and this should not be an issue.

4.9 Forces at the lattice tower bottom

The influence of marine growth on the loads on the foundation piles has been investigated for the FL load case. In Table 4.4, the mean shear force on the piles is given. The mean values for the upwind and the downwind side of the lattice tower are given, as the values were similar. The effect of uniformly distributed marine growth FL0.10 and FL0.20 is also given in the table.

The initial shear forces are very different for the upwind and the downwind side, but the increase, as an absolute value, is similar. Marine growth was applied symmetrically. Therefore, there is no reason to expect the shear force to increase more at a specific pile.

In Table 4.5, the corresponding information is provided for the axial force in the piles. The increase in axial force comes as positives and negatives of the same absolute value. The increased horizontal load on the structure requires an additional vertical force couple in the foundation piles.

For the axial force on the upwind side, the change in axial force is of order of the initial value. In this case, the mean force then changes from compression to tension. This may be very disadvantageous.

The standard deviation of the shear force and the axial force is little influenced by the increased marine growth. The standard deviation of the shear stress increases by less than 2 % for FL0.20. The standard deviation for the axial force increases by less than 5 % for FL0.10 and less than 15 % for FL0.20.

Table 4.4: Mean shear force in the top of the piles.

		Initial value [N]	Change [N]	Relative change [%]
Upwind	MGT=0	1.15 10^6		
	FL0.10		-0.568 10^6	-53.6
	FL0.20		-1.30 10^6	-122.7
Downwind	MGT=0	-8.10 10^6		
	FL0.10		-0.573 10^6	7.07
	FL0.20		-1.31 10^6	16.2

Table 4.5: Mean axial force at the top of the piles. Compression is taken as positive

		Initial value [N]	Change [N]	Relative change [%]
Upwind	MGT=0	7.25 10^4		
	FL0.10		-3.63 10^4	-56.1
	FL0.20		-8.39 10^4	-129.8
Downwind	MGT=0	4.18 10^5		
	FL0.10		3.69 10^4	8.82
	FL0.20		8.53 10^4	20.4

Chapter 5

Summary and conclusions

5.1 Summary

The current standards prescribe a marine growth level of 0.10 m while in the literature, marine growth layers up to 0.20 m thick have been reported for structures in the North Sea. The highest levels are found on structures close to shore, where mussel fouling on the upper 30 m of the structure is dense. However, to reach this level, a period of around seven to eight years is needed. Thus, it may be unnecessary to assume a marine growth thickness of 0.20 m for the entire lifetime.

Marine growth represents an additional non-structural mass and leads to increased wave loading on the structure. The effects of marine growth have been evaluated for a model of the NOWITECH 10 MW reference turbine.

The effects of increasing levels of marine growth on the mode shapes and natural frequencies has been described. Global and 1st bay and 2nd bay local modes were recognized among the twelve first mode shapes. The effect on the first natural frequency was found to be negligible. For the other global-mode natural frequencies, reductions between 7 % and 14 % and between 18 % and 26 % were found for marine growth levels of 0.10 m and 0.20 m respectively. The effect on the 1st bay and 2nd bay local-mode natural frequencies was even larger. A reduction around 24 % and 40 % was found for both groups for marine growth

levels of 0.10 m and 0.20 m respectively.

Because the different relative change in natural frequency, the modes are permuted in their order when sorted by frequency. Still, the mode shapes in general keep their shape when marine growth is applied.

The effect on the mode shapes and natural frequencies when the marine growth was distributed section wise was investigated. Marine growth distributed on a specific bay will affect this bay's local-mode natural frequency. However, applying marine growth on all underwater sections was found to be a conservative approach.

The nP-values were compared with the natural frequencies. The frequencies of 3P and 6P were well separated from the natural frequencies, but one or more natural frequency value was within both the 9P and 12P-ranges for all marine growth levels.

Stress variance spectra have been have been plotted for four reference points and increasing marine growth thickness, to explore the effect of the interference between the nP-values and the natural frequencies. Peaks were recognized at the 3P, 6P and 9P frequencies, as well as at the wave load peak frequency.

The effect of marine growth on the leg normal stress was found negligible. The effect on the in-plane stresses in the bracings was also small. The spectra for the out-of-plane stresses were more sensitive to changes in marine growth. The Fourier amplitudes increased especially much at the nP-values with increasing marine growth thickness. Interference between one or more natural frequency and a nP-value was suggested as reasons for high Fourier amplitudes for certain reference points. However, interference did not affect all reference points in the same way or tho the same extent.

Two "decomposed" analysis setups were proposed, separating the effects of additional mass and the increased diameter. The variance spectra for the out-of-plane stresses from the two "decomposed" analyses were more similar to each other than to the total response. It was seen clearly that the peak at $f \approx 0.15$ Hz was caused by wave loads. In the low frequency range, it would be sufficient to only consider increased diameter to describe the behaviour. For all other frequencies, both the effect from increased diameter and increased mass must be included.

The joint fatigue lifetime was calculated for the X-braces, K-braces and K-legs in the three lowermost sections. For this particular design, the X-brace

fatigue lifetime gave the design value. The X-brace fatigue lifetime showed less sensitivity to changes in marine growth than the K-brace and K-leg lifetime. It was shown that an intermediate thick layer of marine growth may increase the lifetime in some points. Also, the lifetime calculated for the total and the "decomposed models" were compared and as expected, the calculated lifetime was lower when both effects were included.

The influence of marine growth on the loads on the foundation piles was investigated. As the marine growth was applied symmetrically, the increase in load was evenly distributed among the four piles. The standard deviation of the forces was little influenced by the increased marine growth.

5.2 Limitations of the work

In this work, only one specific design was investigated. However, within the lattice tower concept, various structures are imaginable; with varying number of sections, constant or not-constant section height, other member dimensions, additional bracings, etc. It may also be difficult to compare the results from the section wise distributed load cases with results from other structures that are partitioned into more than three sections below the mean water level.

So far, only jacket wind turbine substructures have been installed in the North Sea. This type of structure has not been considered in this report.

Only one specific environmental condition for wind and waves was investigated. The results may have been different for a more severe wind condition. The effects of wave slamming and vortex shedding were not included in the simulations.

Also, a bug in the code resulted in that the initial lifetime for the lattice tower was less than the required 20 years. The bug was detected late in the working process, such that the results were not updated. However, as the change in fatigue lifetime was of interest, not the absolute values as such, it should not have influenced on the discussion.

5.3 Recommendations for further work

The design of the lattice tower was optimized without marine growth before the simulations with marine growth were conducted. A possibility would be to run an iterative optimization process with marine growth included, to see how marine growth influences the lattice tower design. However, the design must still be checked with no marine growth also.

The marine growth level may reach a thickness of 0.10 m after 2-3 years and 0.20 m after 7-8 years. It would be interesting to weigh the results from analyses with 0, 0.10 m and 0.20 m marine growth according to this realistic growth rate.

For this particular design, the X-brace fatigue lifetime was governing for the three lowermost sections, and was less sensitive to changes in marine growth than K-brace and K-leg. It would be very interesting to see the effect of marine growth on a design where the K-brace or K-leg gave the initial design lifetime.

The forces at the lattice tower bottom were affected by the marine growth. This should be investigated further for an environment corresponding to the ultimate limit state.

5.4 Conclusions

Marine growth represents an additional non-structural mass, reducing the structural natural frequencies. Especially for the local-mode natural frequencies, marine growth causes significant reductions; reductions around 24 % and 40 % were found for this design of the lattice tower for a marine growth levels of 0.10 m and 0.20 m respectively.

After investigating the relative importance of the increased hydrodynamic load and additional nonstructural mass, it was concluded that both effects must be included in the model to describe the dynamic behaviour.

For this particular design, the X-brace fatigue lifetime was governing for the three lowermost sections. A maximum reduction in X-brace fatigue lifetime of 44.1 % and 66.8 % for 0.10 m and 0.20 m thick growth. This is a significant reduction in lifetime. Still, the K-braces and K-legs were more sensitive to marine growth.

It was observed that an intermediate layer of marine growth may overestimate the lifetime in certain points. This implies that a design check must be performed also for no marine growth.

It was also observed that joint fatigue lifetime calculated for uniformly distributed marine growth may be non-conservative. Thus, if a cleaning programme is proposed, analyses should be performed with marine growth applied on the parts that are left uncleaned. For analyses of structures in very deep waters, dense marine growth should only be applied down to a realistic depth.

Bibliography

[1] Det Norske Veritas. *Recommended Practice DNV-RP-C203 Fatigue design of offshore steel structures*, April 2010.

[2] D. G. Oldfield, editor. *Appraisal on Marine Fouling on Offshore Structures*, Offshore Technology Paper. Department of Energy, June 1980.

[3] The Norwegian Oil Industry Association (OLF) and The Federation of Norwegian Industry. *NORSOK Standard N-003 Action and action effects*, 2 edition, 2007. Distributed by Standards Norway.

[4] EWEA. The european offshore wind industry key 2011 trends and statistics. Technical report, European Wind Energy Association, 2012.

[5] Michael Muskulus. The full-height lattice tower concept. *Energy Procedia*, 2012. In press.

[6] Anders Kjetså and Lars Jørgen Saaghus. Local Dynamics of Offshore Wind Turbine Jacket Sub-structures. Master's thesis, Norges teknisk-naturvitenskapelige universitet, June 2010.

[7] Fedem Technology AS. FEDEM Windpower. Visited 04-June-2012. `www.fedem.com/en/software/fedem-windpower`.

[8] Ole Gunnar Dahlhaug, Petter Andreas Berthelsen, Trond Kvamsdal, Lars Frøyd, Sverre Skalleberg Gjerde, Zhaoqiang Zhang, Kevin Cox, Eric van Buren, and Daniel Zwick. *Specification of the NOWITECH 10 MW Reference Wind Turbine*. Norwegian Research Centre for Offshore Wind Technology, January 2012.

[9] Haiyan Long and Geir Moe. Truss type support structures for offshore wind turbines. In *Proceedings of European Offshore Wind Conference and Exhibition (EOW 2007)*, Berlin, 2007.

[10] Det Norske Veritas. *Recommended Practice DNV-RP-C205 Environmental conditions and environmental loads*, October 2010.

[11] International Electrotechnical Commission, IEC. *NEK IEC 61400-1 Wind turbines - Part 1: Design requirements*, 3 edition, 2007. Distributed by Standards Norway.

[12] Øivind A. Arntsen, editor. *Compendium in TBA4264 Marine Physical Environment, Waves and Wave Forces.* tapir akademisk forlag, 2007.

[13] W. J. Pierson Jr. and L. Moskowitz. A Proposed Spectral Form for Fully Developed Wind Seas Based on the Similarity Theory of S. A. Kitaigorodskii. *Journal of Geophysical Reseach*, 69(24):5181–5190, 1964.

[14] K. Hasselmann, T. P. Barnett, E. Bouws, H. Carlson, D. E. Cartwright, K. Enke, J. A. Ewing, H. Gienapp, D. E. Hasselmann, P. Kruseman, A. Meerburg, P. Miiller, D. J. Olbers, K. Richter, W. Sell, and H. Walden. Measurements of Wind-Wave Growth and Swell Decay during the Joint North Sea Wave Project (JONSWAP). *Deutsche Hydrographische Zeitschrift*, A:12(8), 1973.

[15] The International Organization for Standarization. *ISO 19902 Petroleum and natural gas industries – Fixed steel offshore structures*, 2007.

[16] The Norwegian Oil Industry Association (OLF) and The Federation of Norwegian Industry. *NORSOK Standard N-004 Design of steel structures*, 2 edition, 2004. Distributed by Standards Norway.

[17] Jan Van der Temple. Offshore Structures: Dynamics and Fatigue. In John Twidell and Gaetano Gaudiosi, editors, *Offshore Wind Power*, chapter 8. Multiscience Publishing Co Ltd., 2009.

[18] European Committee for Standarization. *Eurocode 3: Design of steel structures - Part 1-9:Fatigue*, 2010. Distributed by Standards Norway.

[19] C. Amzallag, J. P. Gerey, J. L. Robert, and J. Bauaud. Standardization of the rainflow counting method for fatigue analysis. *Fatigue*, 16, June 1994.

[20] Tao Yan and Wen Xia Yan. Fouling of Offshore Structures in China – a Review. *Biofouling*, 19, 2003. Supplement.

[21] Simone Dürr and Jeremy C. Thomason, editors. *Biofouling*. Blackwell Publishing Ltd., 2010.

[22] P. Whomersley and G. P. Pickens. Long-term Dynamics of Fouling Communities Found on Offshore Installations in the North Sea. *Journal of the Marine Biological Association of the United Kingdom*, 2003.

[23] Robert Ralph and Robert P. Troake. Marine Growth on North Sea Oil and Gas Platforms. In *Offshore Technology Conference*, 1980.

[24] H. M. Page and D. M. Hubbard. Temporal and Spatial Patterns of Growth in Mussels Mytilus edulis on an Offshore Platform: Relationships to Water Temperature and Food Availability. *Journal of Experimental Marine Biology and Ecology*, 111, 1987.

[25] Iwona B. Beech. Sulfate-reducing bacteria in biofilms on metallic materials and corrosion. *Microbiology Today*, 30, 2003.

[26] IEV Group. The Wave-Driven Marine Growth Preventer. Visited 04-June-2012. `http://www.iev-group.com/index.php?p=contents-item\&id=9536`.

[27] The International Organization for Standarization. *ISO 19901-1 Petroleum and natural gas industries – Specific requirements for offshore structures – Part 1: Metocean design and operating considerations*, 2005.

[28] Iberahin Jusoh and Julian Wolfram. Effects of Marine Growth and Hydrodynamic Loading on Offshore Structures. *Jurnal Mekanikal*, 1996.

[29] N. J. Heaf. The effect of marine growth on the performance of fixed offshore platforms in the north sea. In *Offshore Technology Conference*, 1979.

[30] Fridtjov Irgens. *Formelsamling mekanikk*. tapir akademisk forlag, 3 edition, 2003.

[31] J. Wolfram. The Effect of Marine Growth on Vortex Shedding and Fatigue Life of Tubular Members: Results from a Case Study. In *Proceedings of the 1st International Offshore and Polar Engineering Conference*, Edinburgh, U.K., 1991.

[32] L. R. Wootton. The oscillations of large circular stacks in wind. In *Proceedings of the Institution of Civil Engineers*, volume 43, pages 573–598, 1969.

[33] John H. Nath. Hydrodynamic Coefficients for Macro-Roughnesses. In *Offshore Technology Conference*, 1981.

[34] Cord Böker. *Load simulation and local dynamics of support structures for offshore wind turbines*. PhD thesis, Gottfried Wilhelm Leibniz Universität Hannover, 2009.

[35] Daniel Zwick, Geir Moe, and Michael Muskulus. Iterative optimization approach for the design of full-height lattice towers for offshore wind turbines. *Energy Procedia*, 2012. In press.

[36] Neil Kelley and Bonnie Jonkman. NWTC Design Codes TurbSim. Last modified 03-February-2011. `http://wind.nrel.gov/designcodes/preprocessors/turbsim/`.

[37] Dr. David J. Laino. NWTC Design Codes AeroDyn. Last modified 21-February-2012. `http://wind.nrel.gov/designcodes/simulators/aerodyn/`.

[38] J. Jonkman, S. Butterfield, W. Musial, and G. Scott. Definition of a 5-MW Reference Wind Turbine for Offshore System Development. Technical report, National Renewable Energy Laboratory, 2009.

Appendix A

Numerical study of a simple beam

This appendix gives the extended versions of the Tables 3.1, 3.4 and 3.5 from Section 3.1.

Table A.1: Representative geometric properties of brace and leg members.

Leg members			Brace members		
L [m]	D [m]	T [m]	L [m]	D [m]	T [m]
20	1.0	0.05	30	0.85	0.05
20	0.85	0.05	30	0.65	0.04
20	0.70	0.04	30	0.45	0.03

Table A.2: Change in natural frequencies for simple beam model corresponding to brace members.

L [m]	D [m]	T [m]	MGT [m]	Natural frequency [Hz]	Relative change in n. frequency [%]
30	0.85	0.05	0	16.1	
			0.1	13.6	-15.6 %
			0.2	11.7	-27.3 %
30	0.65	0.04	0	12.3	
			0.1	9.97	-18.9 %
			0.2	8.32	-32.3 %
30	0.45	0.03	0	8.47	
			0.1	6.41	-24.2 %
			0.2	5.11	-39.7 %

Table A.3: Change in drag load according to Morison's formula.

D [m]	MGT [m]	T [s]	dF_D [kN/m]	ΔdF_D [%]	D [m]	MGT [m]	T [s]	dF_D [kN/m]	ΔdF_D [%]
1.00	0.00	7	2.60	0.0	0.70	0.20	9	1.86	111.1
1.00	0.10	7	3.65	40.2	0.70	0.00	12	0.45	0.0
1.00	0.20	7	4.96	90.5	0.70	0.10	12	0.68	50.2
1.00	0.00	9	1.57	0.0	0.70	0.20	12	0.97	116.7
1.00	0.10	9	2.20	40.3	0.60	0.00	7	1.18	0.0
1.00	0.20	9	2.99	90.7	0.60	0.10	7	1.80	52.2
1.00	0.00	12	0.82	0.0	0.60	0.20	7	2.60	120.4
1.00	0.10	12	1.16	41.9	0.60	0.00	9	0.71	0.0
1.00	0.20	12	1.57	93.1	0.60	0.10	9	1.08	52.4
0.85	0.00	7	1.98	0.0	0.60	0.20	9	1.57	121.0
0.85	0.10	7	2.84	43.6	0.60	0.00	12	0.36	0.0
0.85	0.20	7	3.96	99.9	0.60	0.10	12	0.55	54.4
0.85	0.00	9	1.19	0.0	0.60	0.20	12	0.82	126.9
0.85	0.10	9	1.71	43.7	0.45	0.00	7	0.81	0.0
0.85	0.20	9	2.38	100.1	0.45	0.10	7	1.32	61.9
0.85	0.00	12	0.61	0.0	0.45	0.20	7	1.98	143.0
0.85	0.10	12	0.89	45.5	0.45	0.00	9	0.49	0.0
0.85	0.20	12	1.26	104.7	0.45	0.10	9	0.79	62.1
0.70	0.00	7	1.47	0.0	0.45	0.20	9	1.19	143.3
0.70	0.10	7	2.17	48.0	0.45	0.00	12	0.25	0.0
0.70	0.20	7	3.10	110.7	0.45	0.10	12	0.40	64.2
0.70	0.00	9	0.88	0.0	0.45	0.20	12	0.61	149.9
0.70	0.10	9	1.31	48.2					

Appendix B

Element convergence study

This appendix gives the plots that were used to study the convergence of moments in the lattice tower, as described in Section 3.3.

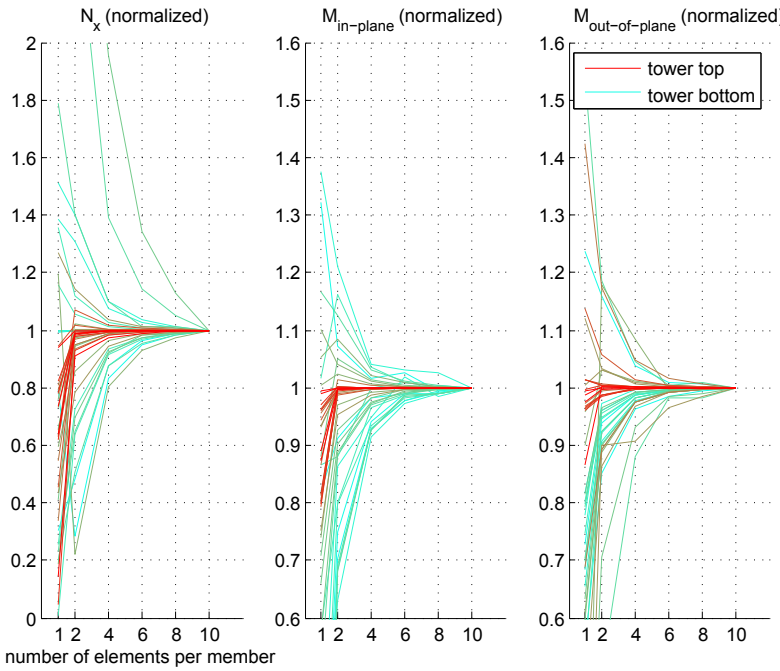

Figure B.1: Convergence of axial force and moments for K-braces.

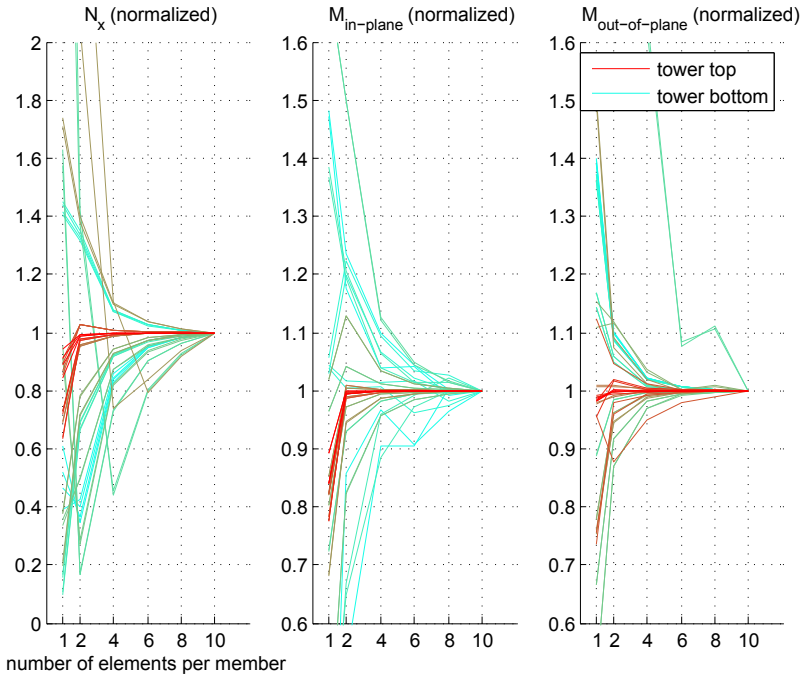

Figure B.2: Convergence of axial force and moments for X-braces.

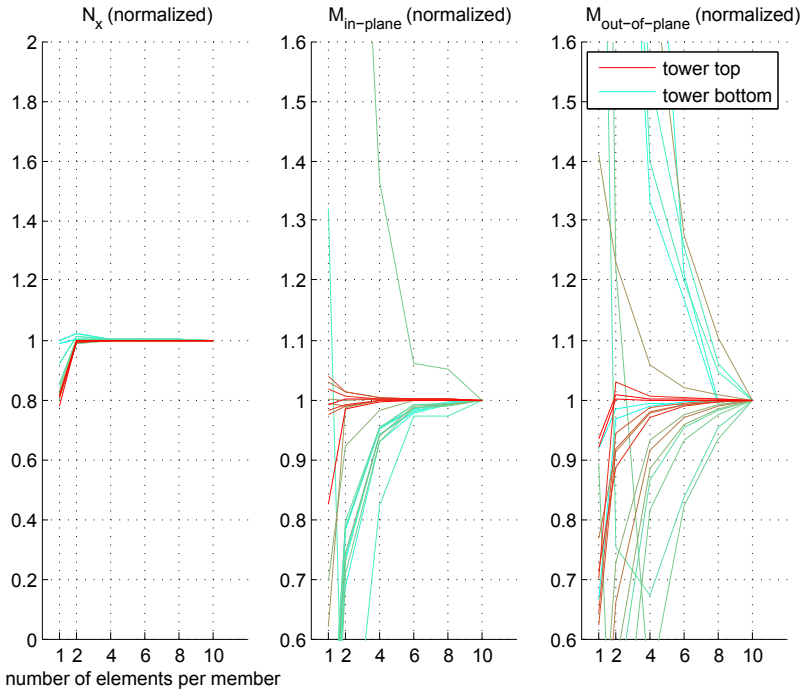

Figure B.3: Convergence of axial force and moments for K-legs.

Appendix C

Natural frequencies of the lattice tower

This appendix gives the extended versions of the Tables 4.2 and 4.3 from Section 4.3. Here, the natural frequencies for the 1st and 2nd bay local modes have not been averaged.

Table C.1: Change in natural frequencies for the FL load cases.

Mode label	Relative change in natural frequency [%] FL0.05	FL0.10	FL0.15	FL0.20
A	-0.03	-0.10	-0.18	-0.27
B	-2.96	-6.78	-11.5	-18.2
C	-12.8	-25.0	-34.3	-41.6
D	-12.6	-24.6	-33.6	-39.6
E	-12.6	-24.8	-34.1	-41.4
F	-4.43	-9.03	-13.8	-18.4
G	-7.72	-14.3	-20.4	-26.0
H	-13.3	-24.9	-33.9	-41.1
I	-12.4	-23.0	-31.2	-37.7
J	-12.8	-24.4	-33.4	-40.6
K	-12.2	-21.2	-28.5	-34.6
L	-15.6	-26.5	-35.0	-41.9

Table C.2: Change in natural frequencies for the SEC load cases. 0.10 m marine growth thickness.

Mode label	Relative change in natural frequency [%] SEC3	SEC2+3	FL0.10	SEC1+2	SEC1
A	-0.10	-0.12	-0.13	-0.03	0.00
B	-4.24	-6.56	-6.92	-2.98	-0.47
C	-0.58	-13.2	-27.5	-27.5	-27.1
D	-0.07	-8.69	-27.3	-27.3	-27.2
E	-0.01	-5.02	-27.5	-27.5	-27.5
F	-4.71	-8.31	-8.89	-4.69	-0.63
G	-8.21	-12.9	-13.5	-6.85	-0.68
H	-7.78	-15.3	-26.5	-25.9	-0.77
I	-4.63	-16.7	-24.0	-23.9	-0.29
J	–	-22.3	-26.3	-26.1	-0.33
K	-14.8	-19.8	-20.0	-6.31	-1.12
L	-18.5	-25.3	-25.4	-1.95	-0.24

Appendix D

Spectra for out-of-plane displacement

This appendix gives the variance spectra for the out-of-plane displacement in PRX1 and RPX3. The red vertical lines represent the ranges of the nP-values, as explained in Section 4.4.

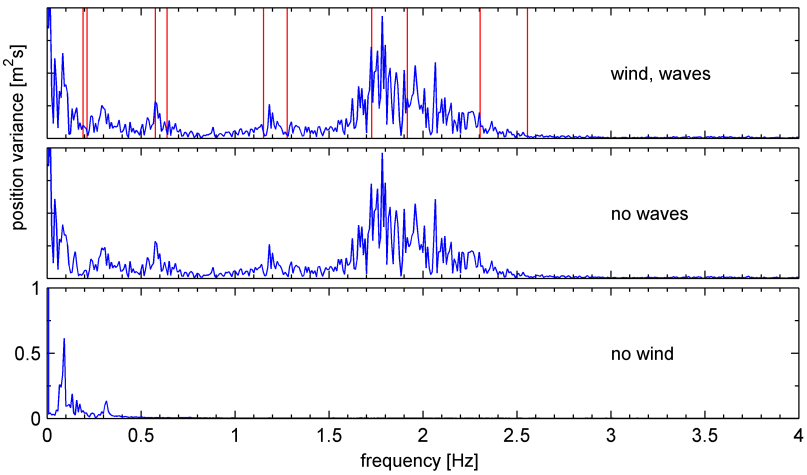

Figure D.1: Variance spectrum for out-of-plane displacement of RPX1.

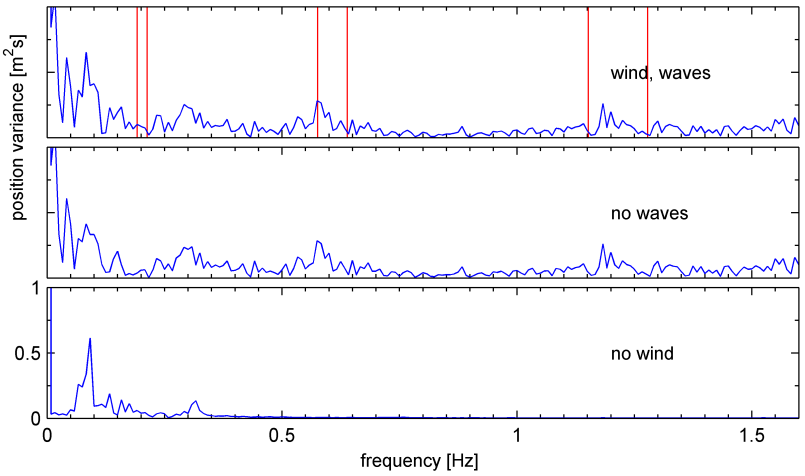

Figure D.2: Variance spectrum for out-of-plane displacement of RPX1.

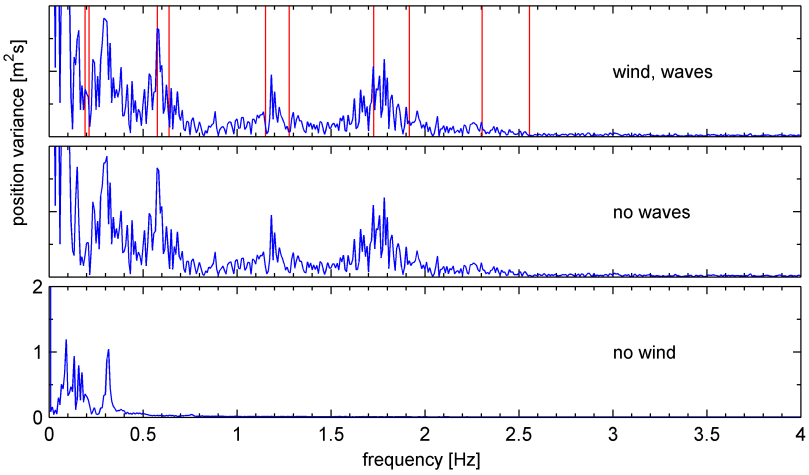

Figure D.3: Variance spectrum for out-of-plane displacement of RPX3.

Appendix E

Stress variance spectra

This appendix gives the stress variance spectra for the various reference plots, as described in Section 4.6. The red vertical lines represent the ranges of the nP-values, as explained in Section 4.4.

E.1 Normal stresses

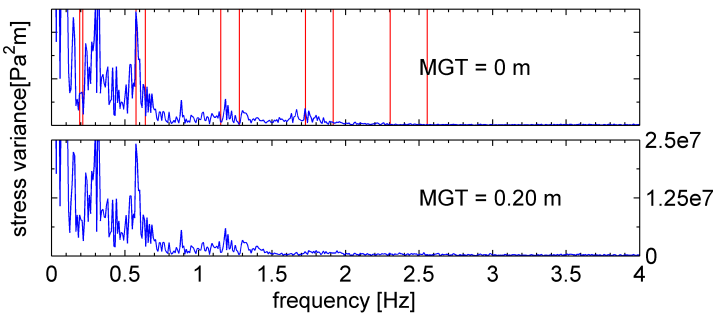

Figure E.1: Variance spectrum for leg normal stress in RPK1.

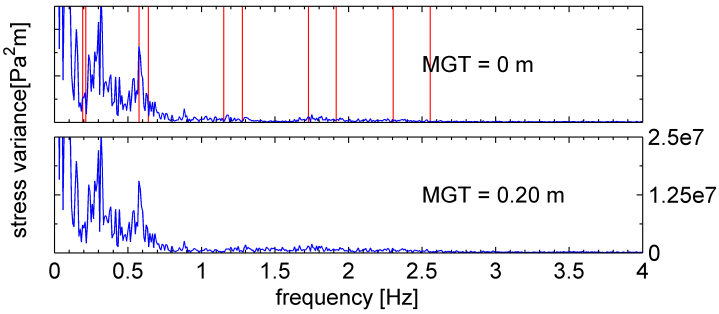

Figure E.2: Variance spectrum for leg normal stress in RPK3.

E.2 In-plane stresses

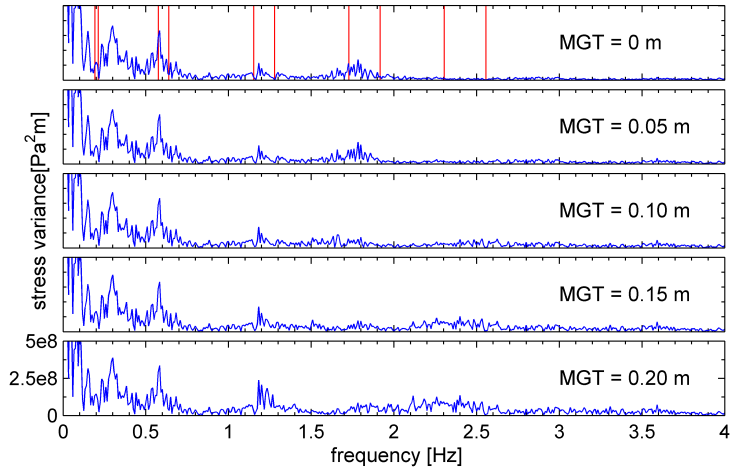

Figure E.3: Variance spectrum for brace in-plane stresses in RPK1.

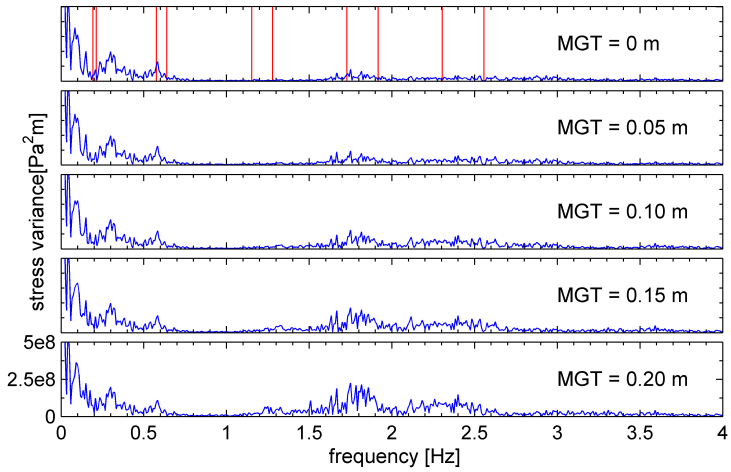

Figure E.4: Variance spectrum for brace in-plane stresses in RPK3.

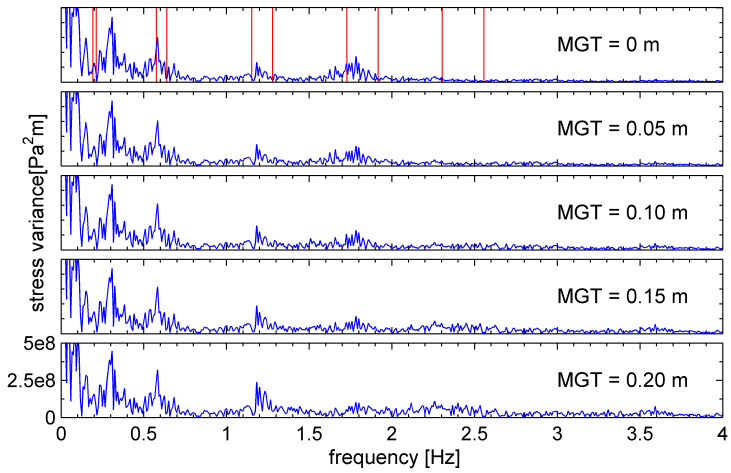

Figure E.5: Variance spectrum for brace in-plane stresses in RPX1.

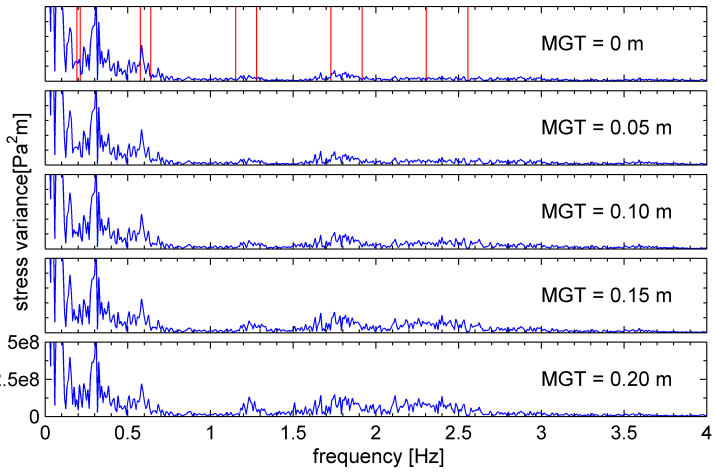

Figure E.6: Variance spectrum for brace in-plane stresses in RPX3.

E.3 Out-of-plane stresses

The results for the group of simulations where only the increased member diameter was taken into account are plotted in *green*. The results when only the additional mass of the marine growth was included are plotted in *red*.

Blue lines represent the results from the analyses where both effects are included. Note that for the plots labelled with *Blue: MGT=0*, the result for no marine growth is plotted as reference in blue.

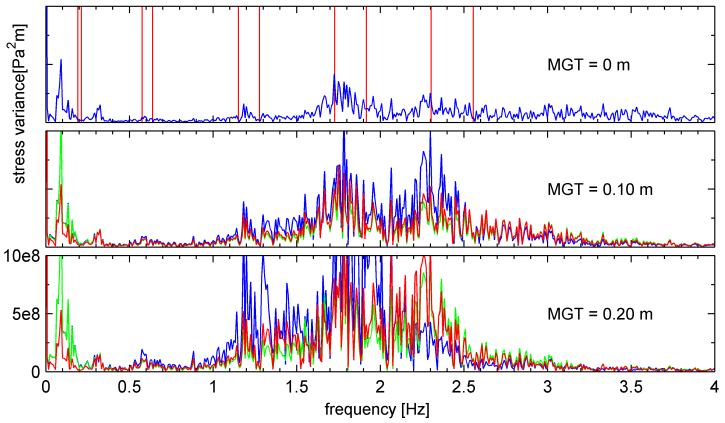

Figure E.7: Variance spectrum for brace out-of-plane stresses in RPK1.

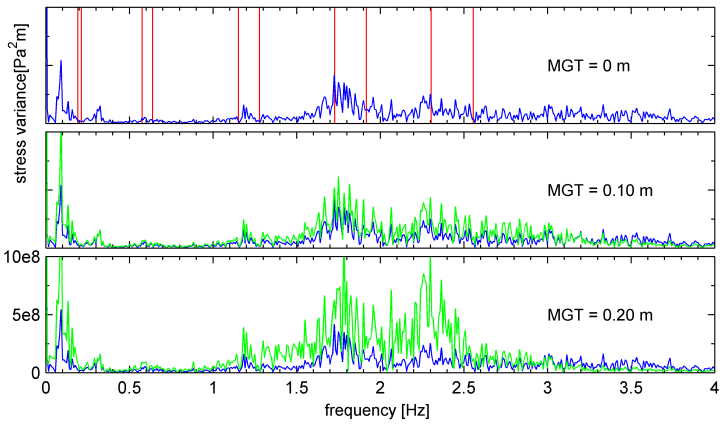

Figure E.8: Variance spectrum for brace out-of-plane stresses in RPK1. Blue: MGT=0.

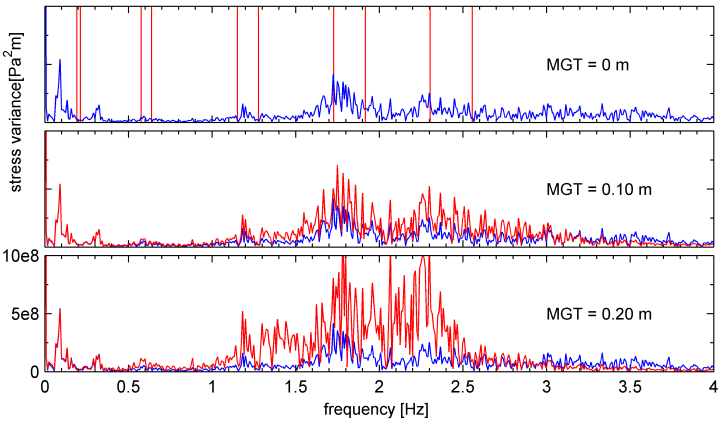

Figure E.9: Variance spectrum for brace out-of-plane stresses in RPK1. Blue: MGT=0.

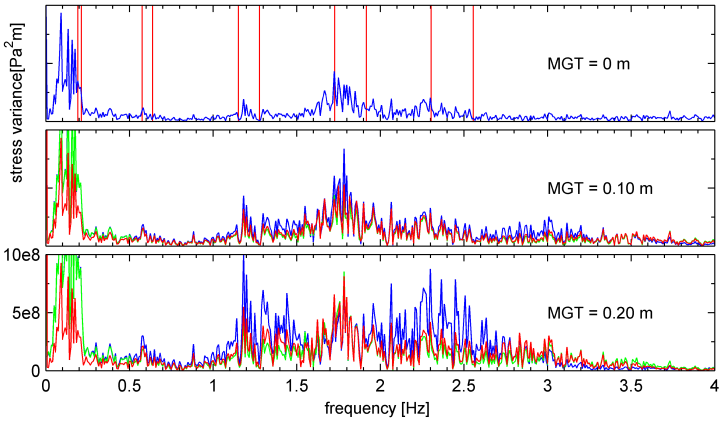

Figure E.10: Variance spectrum for brace out-of-plane stresses in RPK3.

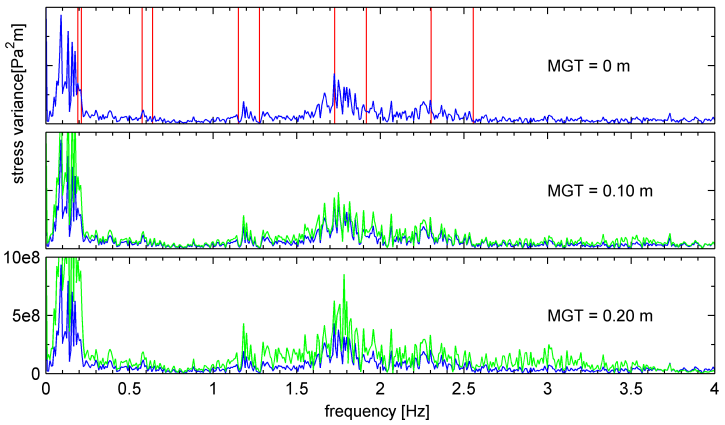

Figure E.11: Variance spectrum for brace out-of-plane stresses in RPK3. Blue: MGT=0.

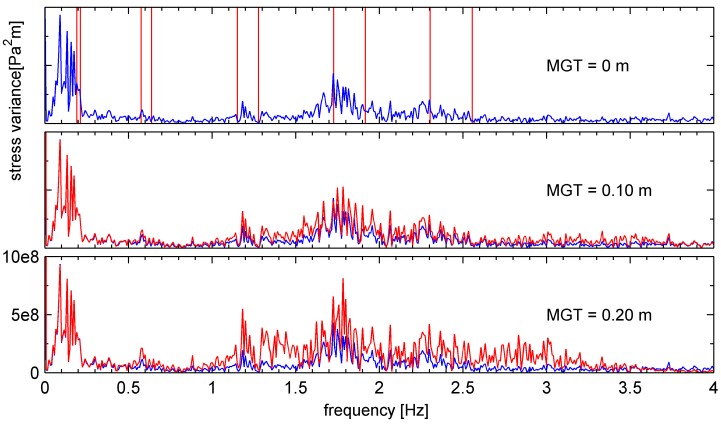

Figure E.12: Variance spectrum for brace out-of-plane stresses in RPK3. Blue: MGT=0.

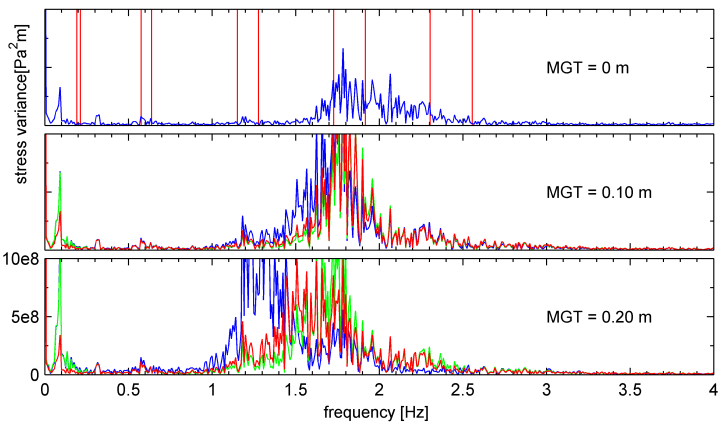

Figure E.13: Variance spectrum for brace out-of-plane stresses in RPX1.

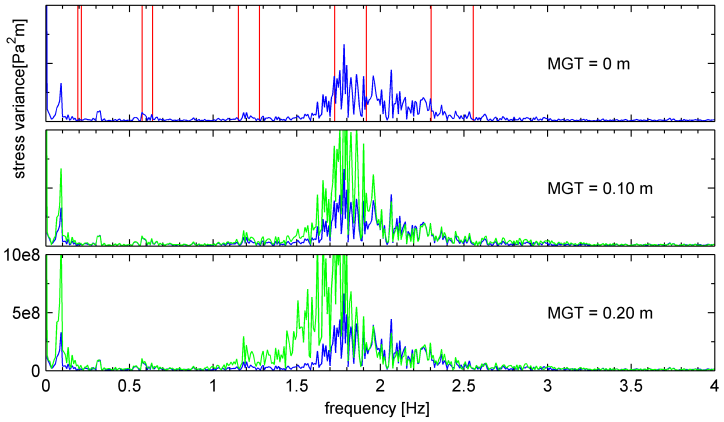

Figure E.14: Variance spectrum for brace out-of-plane stresses in RPX1. Blue: MGT=0.

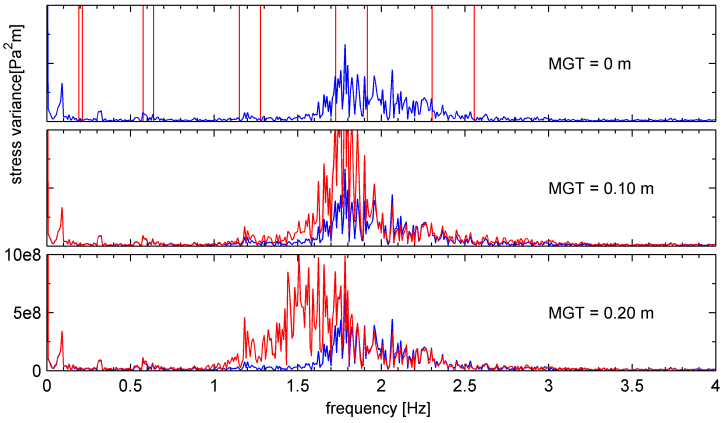

Figure E.15: Variance spectrum for brace out-of-plane stresses in RPX1. Blue: MGT=0.

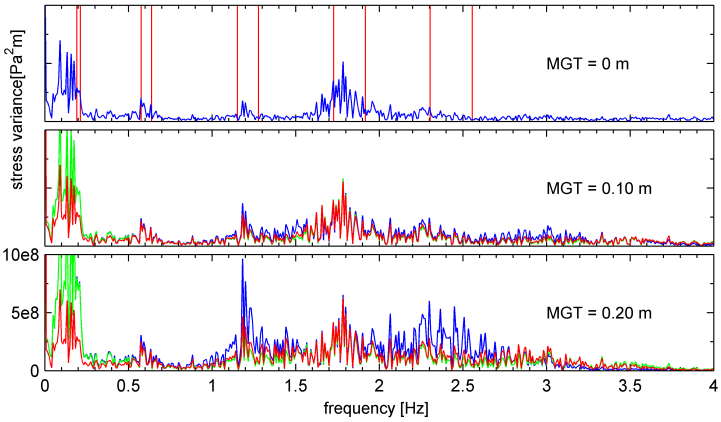

Figure E.16: Variance spectrum for brace out-of-plane stresses in RPX3.

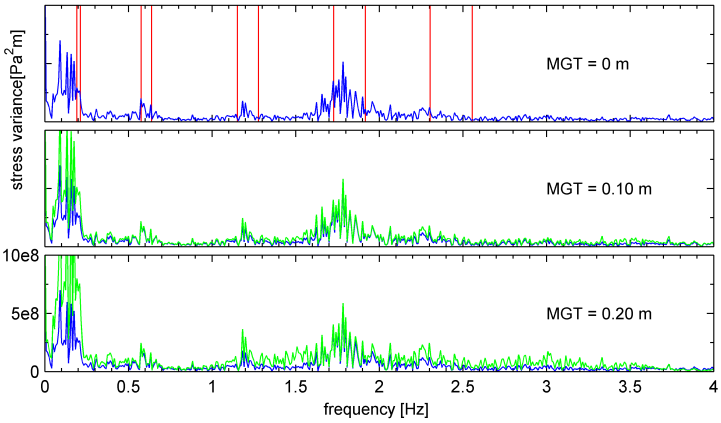

Figure E.17: Variance spectrum for brace out-of-plane stresses in RPX3. Blue: MGT=0.

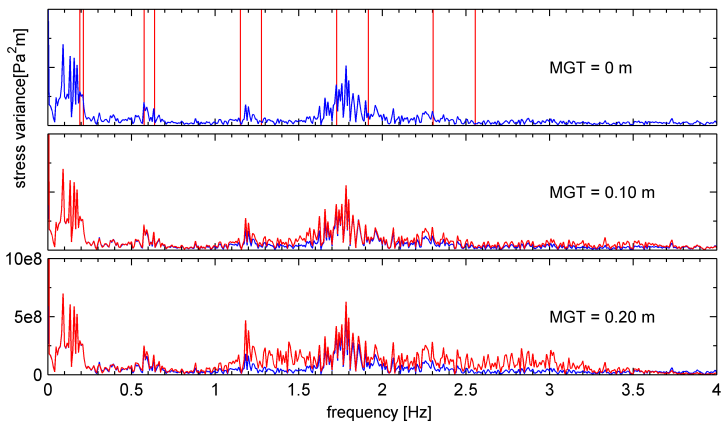

Figure E.18: Variance spectrum for brace out-of-plane stresses in RPX3. Blue: MGT=0.